NATIONAL TECHNICAL UNIVERSITY OF ATHENS
SCHOOL OF CIVIL ENGINEERING
LABORATORY FOR EARTHQUAKE ENGINEERING

Seismic risk assessment of frame structures using stochastic beam-column elements

A dissertation submitted in partial satisfaction
of the requirements for the degree

MSc in Analysis & Design of Earthquake Resistant Structures

by Georgios A. Balokas

June 2016

Supervisor:
Dr. Michalis Fragiadakis
Assistant Professor NTUA

Seismic risk assessment of frame structures using stochastic beam-column elements

MSc in Analysis and Design of Earthquake Resistant Structures

A dissertation by:

Georgios A. Balokas

Dipl (School of Applied Mathematical & Physical Sciences, NTUA) 2010
Dipl (School of Civil Engineering, NTUA) 2013

Supervisor:
Dr. Michalis Fragiadakis
Assistant Professor NTUA

Research topics:
Stochastic finite elements
Earthquake engineering
Reliability analysis

National Technical University of Athens
School of Civil Engineering
Laboratory for Earthquake Engineering
Athens, Greece

2016

Preface

This master's dissertation was conducted and written at the Laboratory for Earthquake Engineering of the School of Civil Engineering, at the National Technical University of Athens (NTUA). It is a result of nearly a year's work and finalizes my Master of Science studies in Structural Engineering, emphasizing on advanced methods of computational engineering and reliability analysis. This work was supervised closely from the beginning until its very end, by the Assistant Professor of the Laboratory for Earthquake Engineering of NTUA, Dr. Michalis Fragiadakis.

Acknowledgments

This dissertation is the last step for obtaining the MSc degree in Structural Engineering at the National Technical University of Athens. I would like to express my deepest gratitude to my supervisor Michalis Fragiadakis, for giving me the opportunity to work with him on such an interesting topic. Our collaboration was ideal and I can only feel beneficiary from the whole experience. I would also like to especially express my appreciation for his support on the decisions I made during this time concerning my future and state that his insight and guidance prepared me for the next step and made me a better researcher.

Special thanks to my current supervisor Dr. Steffen Czichon, for offering me the opportunity to work abroad on the FULLCOMP project and the flexibility I needed in order to finalize my thesis.

Last but not least, I would like to thank my family (Tasos, Sofia and Sotiris) and friends for encouraging me, supporting me but also enduring me all these years of my academic career.

Table of Contents

Abstract

A novel modeling for the assessment of structures with uncertain, spatially variable system properties is presented. The use of flexibility-based (or force-based) fiber elements for structures whose properties are described by homogeneous non-Gaussian translation fields is discussed. For deterministic problems, force-based fiber elements have been proven able to provide accurate response estimates using a single beam element per structural member. The proposed modeling allows using different integration schemes depending on the correlation length parameter of the field and is able to consistently integrate the spatial variability of the uncertain system properties. This formulation allows to overcome the need for a very dense mesh of beam elements and considerably reduces the computing effort, even for stochastic fields of short correlation length and for highly nonlinear problems. The performance of the proposed modeling is demonstrated on a steel portal frame and on a reinforced concrete bridge and is assessed by using the Monte Carlo Simulation under the assumption of a pre-defined power spectral density function of the stochastic fields. Nonlinear static analysis offers probabilistic capacity curves that provide valuable information on the sensitivity of the proposed modeling with respect to the correlation length (correlation scale) of the stochastic fields and its effect on the system response variability and reliability. Furthermore, a series of nonlinear response history analyses are performed using natural ground motions of levels of increasing seismic intensity and subsequently used for calculating the bridge's system fragility. The dissertation underlines the importance of realistic uncertainty quantification and provides a valuable guidance for the nonlinear stochastic analysis of skeletal structures.

Extended summary (in Greek)

Η μέθοδος των στοχαστικών πεπερασμένων στοιχείων γνωρίζει μεγάλη άνθιση τα τελευταία 25 χρόνια. Οι έμφυτες αβεβαιότητες σε όρους υλικών, γεωμετρίας και φορτίσεων των κατασκευών έχουν φέρει τις πιθανοτικές μεθόδους ανάλυσης στο προσκήνιο, καθώς τα ντετερμινιστικά προσομοιώματα αγνοούν σημαντικές παραμέτρους αναφορικά με την πραγματική απόκριση ενός δομήματος. Μικρές διακυμάνσεις κάποιων ιδιοτήτων μπορούν να δημιουργήσουν μεγάλες αποκλίσεις στην απόκριση και συνολικά στην αξιοπιστία της κατασκευής.

Οι πλαισιωτές κατασκευές έχουν μελετηθεί υπολογιστικά στο πλαίσιο πιθανοτικών αναλύσεων με πολλές μεθόδους και παραλλαγές. Πεπερασμένα στοιχεία 2 και 3 διαστάσεων έχουν χρησιμοποιηθεί για την λεπτομερέστερη περιγραφή των διακυμάνσεων των στοχαστικών πεδίων, παρά το μεγάλο υπολογιστικό κόστος. Ο συνδυασμός αυτών των στοιχείων με δυναμικές αναλύσεις (χρονοιστορίες) καθιστά τις μεθόδους ακατάλληλες για εφαρμογές σε πραγματικές κατασκευές μεγάλης κλίμακας. Το ραβδωτό πεπερασμένο στοιχείο μετατοπίσεων (*displacement-based beam-column element*) μπορεί να βρεθεί σε εφαρμογές στοχαστικών αναλύσεων, όμως η πυκνή διακριτοποίηση που χρειάζεται για ακριβείς υπολογισμούς αυξάνει το υπολογιστικό κόστος. Η παρούσα εργασία μελετά την εφαρμογή των ραβδωτών στοιχείων δυνάμεων (*force-based beam-column element*) στην μέθοδο των στοχαστικών πεπερασμένων στοιχείων. Σε ντετερμινιστικές αναλύσεις το συγκεκριμένο στοιχείο προσφέρει εξαιρετική ακρίβεια με ένα μόνο στοιχείο σε κάθε μέλος. Μελετάται η συμπεριφορά του σε όρους ακρίβειας και κόστους σε στατικές και δυναμικές στοχαστικές αναλύσεις.

Στο πρώτο κεφάλαιο γίνεται μία σύνοψη των πιο πρόσφατων σχετικών μελετών (*state of the art*) καθώς και σχολιασμός γύρω από την ερευνητική δραστηριότητα στο τομέα των στοχαστικών υπολογιστικών μεθόδων για πλαισιωτές κατασκευές.

Στο δεύτερο κεφάλαιο παρουσιάζονται οι βασικές θεωρητικές αρχές των ραβδωτών στοιχείων διανεμημένης πλαστικότητας ή στοιχείων ινών (*distributed plasticity elements or fiber beam-column elements*). Αποσαφηνίζονται οι διαφορές από τα κλασσικά ραβδωτά στοιχεία συγκεντρωμένης πλαστικότητας όπως επίσης και οι διαφορές μεταξύ του στοιχείου δυνάμεων και του στοιχείου μετατοπίσεων.

Αναφέρονται συνοπτικά οι βασικές σχέσεις των στοιχείων ινών, από τις κινηματικές θεωρήσεις και το σωματόδετο σύστημα συντεταγμένων μέχρι και την έκφραση του μητρώου δυσκαμψίας για τα δύο διαφορετικά στοιχεία.

Στο τρίτο κεφάλαιο παρουσιάζονται συνοπτικά οι βασικότερες αρχές της μεθόδου των στοχαστικών πεπερασμένων στοιχείων. Ξεκινώντας από τον ορισμό των στοχαστικών πεδίων/διαδικασιών, αναφέρονται οι διάφοροι τρόποι διακριτοποίησης όπως επίσης και οι δημοφιλέστερες μέθοδοι υπολογισμού της μεταβλητότητας της απόκρισης. Στην εργασία χρησιμοποιούνται προσομοιώσεις *Monte Carlo* για τον υπολογισμό των αποτελεσμάτων και κατόπιν στατιστική επεξεργασία των εξαγόμενων δειγμάτων. Έμφαση δίνεται στους τρόπους παραγωγής των στοχαστικών πεδίων με Κανονική κατανομή και στη μετάβαση μέσω μετασχηματισμών σε πεδία με μη Κανονική κατανομή.

Στο τέταρτο κεφάλαιο αναπτύσσεται αναλυτικά η προτεινόμενη μεθοδολογία της εργασίας. Παρουσιάζονται οι σχέσεις που περιγράφουν την διάδοση της αβεβαιότητας μέσα στο στοιχείο δυνάμεων μέχρι την παραγωγή του στοχαστικού μητρώου δυσκαμψίας. Με την προτεινόμενη μεθοδολογία μπορούν να εφαρμοστούν διάφορες μέθοδοι αριθμητικής ολοκλήρωσης, με την μέθοδο *Gauss-Lobatto* να προτιμάται ως καταλληλότερη. Ο αριθμός των σημείων ολοκλήρωσης στο πεπερασμένο στοιχείο είναι κομβικός για την μέθοδο, καθώς χαρακτηρίζει την περιγραφή του στοχαστικού πεδίου και κατά συνέπεια την ακρίβεια της μεθόδου. Ακόμη, παρουσιάζεται αναλυτικά η εφαρμογή της μεθόδου και ο προγραμματισμός σε Η/Υ μέσω των προγραμμάτων *MATLAB* και *OpenSees*, με κομμάτια κώδικα και επεξηγήσεις.

Το πέμπτο κεφάλαιο περιέχει την εφαρμογή της προτεινόμενης μεθόδου σε ένα διδιάστατο, δίστυλο, μεταλλικό πλαίσιο. Οι ιδιότητες του χάλυβα θεωρείται ότι περιγράφονται από στοχαστικά πεδία λογαριθμοκανονικής κατανομής σε κάθε μέλος. Το πλαίσιο υποβάλλεται σε μη γραμμική στατική ανάλυση και σε μη γραμμική ανάλυση χρονοιστορίας. Τα αποτελέσματα των αναλύσεων συγκρίνονται με αναλύσεις του κλασικού στοιχείου μετατοπίσεων με πυκνή διακριτοποίηση. Σε όλο το κεφάλαιο παρουσιάζονται και παραμετρικές αναλύσεις για το μήκος συσχέτισης (*correlation length*) των στοχαστικών πεδίων. Με τον κατάλληλο αριθμό σημείων ολοκλήρωσης η σύγκλιση είναι ικανοποιητική, ενώ εξάγονται σημαντικά συμπεράσματα για την

αλληλεπίδραση της στοχαστικότητας με την μη γραμμικότητα. Το υπολογιστικό κόστος μειώνεται εντυπωσιακά, ειδικά στην δυναμική ανάλυση. Το γεγονός αυτό καθιστά τη μέθοδο εφαρμόσιμη σε κατασκευές μεγάλης κλίμακας.

Στο έκτο κεφάλαιο γίνεται εφαρμογή της μεθόδου σε γέφυρα από οπλισμένο σκυρόδεμα με σκοπό την εξαγωγή των καμπυλών τρωτότητας. Ο φορέας είναι εμπνευσμένος από την Γέφυρα του Αράχθου στην Εγνατία Οδό. Οι ιδιότητες του οπλισμένου σκυροδέματος των βάθρων θεωρείται ότι μεταβάλλονται βάσει στοχαστικών πεδίων. Για την εξαγωγή των καμπυλών τρωτότητας χρησιμοποιούνται μη γραμμικές δυναμικές αναλύσεις με 15 σεισμικές καταγραφές και προσομοιώσεις *Monte Carlo*. Πραγματοποιείται παραμετρική ανάλυση για το μήκος συσχέτισης των πεδίων, ενώ γίνεται και σχολιασμός για την επιλογή των μηχανικών παραμέτρων απόκρισης (*engineering demand parameters*) σε μία ανάλυση τρωτότητας.

Στο έβδομο κεφάλαιο συνοψίζονται τα βασικότερα συμπεράσματα της εργασίας και της προτεινόμενης μεθόδου. Ακολουθούν οι βιβλιογραφικές αναφορές που αποτελούν έναν καλό οδηγό για μελέτη παρόμοιων ερευνητικών θεμάτων. Ακόμη, περιέχεται παράρτημα με χρήσιμες εφαρμογές και πληροφορίες που χρησιμοποιήθηκαν στην εργασία, όπως πίνακες κανόνων αριθμητικής ολοκλήρωσης, προγραμματισμός της αριθμητικής ολοκλήρωσης *Gauss-Lobatto,* προγραμματισμός της μεθόδου φασματικής απεικόνισης για την παραγωγή στοχαστικών πεδίων Γκαουσιανής κατανομής και κώδικας σε γλώσσα *Tcl* για το πρόγραμμα *OpenSees* με εφαρμογή της προτεινόμενης μεθόδου για μία στοχαστική, στατική, μη γραμμική ανάλυση πλαισίου.

List of Figures

List of Tables

- This page was left intentionally blank -

1. Introduction

The stochastic approach is a valuable a tool for the probabilistic assessment of structures. The inherent randomness, e.g. in material, geometry and loads, hampers the deterministic treatment of the problem, while often a small variation of a system property can affect considerably the response. Beam theory is appropriate for the assessment of many structural analysis problems, and is certainly the most popular choice for the performance assessment of inelastic frame structures. However, the use of beam elements for the stochastic assessment of inelastic problems is rather limited, since most researchers prefer other modelling choices.

Most and Bucher (2006, 2007) proposed using a 2D and a 3D discretization for the stochastic assessment of beams. Their approach offers a more detailed description of the stochastic fields, but the computational resources required obstruct the extension of the method to full-scale buildings. A 2D model for the stochastic assessment of beam problems is also used for reinforced concrete structures in Vasconcellos *et al.* (2003). Especially when dynamic loads are applied, the use of higher order finite elements is prohibitive. The computing cost also depends on the algorithm that will be adopted for solving the stochastic problem. Despite the many extensive efforts on the development of analytical methods, the Monte Carlo simulation method (MCS) (Shinozuka, 1972) remains the most reliable option, despite its increased cost. The use of efficient finite element modeling is, therefore, critical for the successful application of the stochastic method.

Fiber elements have been used on several occasions for the reliability assessment of frame structures. Contrary to the deterministic problem, where inelastic deformations are lumped at the beam ends, in stochastic analysis we need distributed plasticity elements so that our calculations consider the variation of system properties along the

member. One of the early efforts using fiber elements was that of Lee and Mosalam (2003) who introduced a stochastic fiber-element model for the assessment of RC structures. Their work is based on common displacement-based elements and hence requires significant computing resources.

The use of force-based fiber beam-column elements, allows to consistently integrate the spatial variability of inelastic systems with uncertain system properties. For deterministic problems these elements are able to provide accurate response estimates using a single beam element per member. The use of force-based elements for the stochastic assessment of steel frames was first presented in Stefanou and Fragiadakis (2009) where the seismic capacity of a steel frame subjected to several natural ground motion records was examined. Hamutcuoglu and Scott (2009) used the force-based formulation for the reliability assessment of bridges under moving loads, while Feng and Li (2015) used force-based fiber elements for the stochastic nonlinear static assessment of a simple two-bay reinforced concrete frame.

This study proposes a novel modeling for the dynamic seismic assessment of structural systems within the stochastic finite element method. The proposed modeling is able to consistently integrate the spatial variability of the uncertain system properties on frame structures, using a force-based fiber beam-column element. Previous work has proven the ability of this element to provide accurate estimates of nonlinear behavior using a single beam element per structural member. By using a variation of the integration point method, the fluctuation of the stochastic field is adequately described within the member. Once the proposed element formulation is implemented in a computer code, the user is able to adopt different integration schemes and a varying order of integration, having full control and considerably reducing the computing cost without compromising the accuracy, even for stochastic fields of very small correlation lengths.

Homogeneous non-Gaussian translation stochastic fields are generated to describe the modeling uncertainties in a realistic way. The performance of the method is demonstrated on a steel portal frame under both static and dynamic nonlinear analysis. As reference solution, we consider models that use a very dense mesh of displacement-based fiber beam-column elements. The response variability is assessed with the aid of

the Monte Carlo simulation under the assumption of a pre-defined spectral density function. Furthermore, the proposed modeling is implemented on a real-scale reinforced concrete bridge structure to assess the fragility and highlight the importance of realistic uncertainty quantification. A parametric investigation is carried out throughout the whole study regarding the spectral characteristics of the provided stochastic fields and their influence on the response variability.

2. Fiber beam-column elements

Contrary to plastic-hinge beam-column elements, where inelastic demand is lumped at the beam ends, distributed plasticity elements allow yielding to occur at any location along the element. The two most common formulations of distributed plasticity elements are the displacement-based (DB) and the force-based (FB) approach.

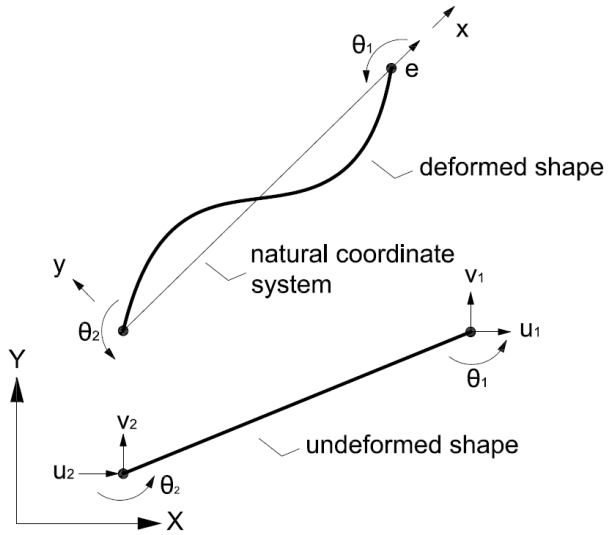

Figure 1: Cartesian and natural coordinates of a plane beam-column element.

Displacement-based elements, also known as stiffness-based elements, follow the classical finite element theory and use cubic Hermitian shape functions to interpolate the displacement field. These elements require a fine mesh at the regions where inelastic deformations are expected to be high, e.g. the beam ends. On the other hand, force-based elements (Zeris and Mahin 1988, Spacone *et al*. 1996, Neuenhofer and Filippou 1998) use force interpolation functions to overcome the problem of the unknown curvature distribution once yielding occurs. This approach always maintains equilibrium of both forces and deformations and converges to a state that satisfies the constitutive

laws within a specified tolerance. For deterministic problems a single force-based element per member is sufficient for accurately predicting the nonlinear behavior, provided that no element loads are present.

Nonlinear beam-column elements are usually based on the "natural" coordinate system (also known as "basic" or "corotational" system). This system translates and rotates following the motion of the element. The beam element has three degrees-of-freedom (Figure 1), the axial displacement e and two rotations θ_1 and θ_2 which fully describe the inelastic demand and are grouped in: $\mathbf{v} = [e, \theta_1, \theta_2]^{\mathrm{T}}$. Following the Euler-Bernoulli beam theory, the strain $\varepsilon_x(x,y)$ is obtained as:

$$\varepsilon_x(x,y) = \begin{bmatrix} 1 & -y \end{bmatrix} \begin{bmatrix} \varepsilon_0(x) \\ k(x) \end{bmatrix} = \mathbf{a}_S(y)\,\mathbf{d}_{\mathrm{sec}}(x) \tag{1}$$

where $\mathbf{a}_s(y)$ is the section kinematic matrix and $\mathbf{d}_{\mathrm{sec}}(x)$ is the section deformation vector. The section stiffness matrix is calculated as the derivative of the section forces $\mathbf{D}_{\mathrm{sec}}$ with respect to the section deformations $\mathbf{d}_{\mathrm{sec}}$:

$$\mathbf{k}_{\mathrm{sec}} = \frac{\partial \mathbf{D}_{\mathrm{sec}}}{\partial \mathbf{d}_{\mathrm{sec}}} = \frac{\partial \mathbf{D}_{\mathrm{sec}}}{\partial \sigma}\frac{\partial \sigma}{\partial \varepsilon}\frac{\partial \varepsilon}{\partial \mathbf{d}_{\mathrm{sec}}} = \int_A \mathbf{a}_S \frac{\partial \sigma}{\partial \varepsilon}\mathbf{a}_S^{\mathrm{T}} dA = \int_A \frac{\partial \sigma}{\partial \varepsilon}\begin{bmatrix} 1 & -y \\ -y & y^2 \end{bmatrix} dA \tag{2}$$

where $\partial\sigma/\partial\varepsilon$ is the tangent of the nonlinear uniaxial constitutive law and y is the distance from the neutral axis. Distributed plasticity elements are also known as "fiber" elements, since each section is discretized to a finite number of fibers which are used to numerically calculate the section stiffness $\mathbf{k}_{\mathrm{sec}}$ of Eq. (2). If N is the axial force and M is the bending moment of the cross-section, the section forces are calculated by integrating the section stresses:

$$\mathbf{D} = \begin{bmatrix} N \\ M \end{bmatrix} = \int_A \begin{bmatrix} 1 \\ -y \end{bmatrix} \sigma_x dA = \int_A \mathbf{a}_S^{\mathrm{T}} \sigma_x dA \tag{3}$$

2.1. Displacement-based fiber elements

The DB method interpolates the displacements of the element and the relationship between section and element deformations is given by:

$$\mathbf{d}_{\mathrm{sec}} = \mathbf{B}_N(x)\mathbf{v} = \frac{1}{L}\begin{bmatrix} 1 & 0 & 0 \\ 0 & 2(3x/L-2) & 2(3x/L-1) \end{bmatrix}\mathbf{v} \tag{4}$$

where $\mathbf{B}_N(x)$ is the strain-displacement transformation matrix of the element. The element stiffness matrix is first calculated in the natural system as:

$$\mathbf{K}_{\mathrm{N}} = \int_L \mathbf{B}_{\mathrm{N}}^{\mathrm{T}} \mathbf{k}_{\mathrm{sec}} \mathbf{B}_{\mathrm{N}} dL \tag{5}$$

The global element stiffness matrix is obtained from $\mathbf{K}_{\mathrm{N}}$ with the aid of simple algebraic transformations (Fragiadakis, 2016).

2.2. Force-based fiber elements

Force-based elements use force interpolation functions, which are always exact since the distribution of bending moment remains linear after element yielding. The force interpolation matrix $\mathbf{b}_{\mathrm{S}}$ relates section forces with the natural forces **S**, thus:

$$\mathbf{D}_{\mathrm{sec}} = \mathbf{b}_{\mathrm{S}}\mathbf{S} \Leftrightarrow \mathbf{D}_{\mathrm{sec}} = \begin{bmatrix} 1 & 0 & 0 \\ 0 & x/L-1 & x/L \end{bmatrix} \mathbf{S} \tag{6}$$

The natural stiffness matrix is calculated as the inverse of the element flexibility matrix as:

$$\mathbf{K}_N^{-1} = \mathbf{F}_N = \int_L \mathbf{b}_S^T \left(\mathbf{k}_{\mathrm{sec}}\right)^{-1} \mathbf{b}_S \, dL \tag{7}$$

The element stiffness matrix is calculated numerically using Gauss-Lobatto integration. Gauss-Lobatto integration is a variation of Gauss integration that considers the beam ends as integration sections, where the bending moment receives its maximum values. The flexibility formulation does not allow calculating directly the internal forces of the element. To overcome this, an additional iterative process at the element level, known as "element-state" determination process is introduced (Ciampi and Carlesimo 1986, Spacone *et al*, 1996).

The first step of the iterative procedure is to determine the vector of the natural forces from the vector of the nodal Cartesian displacements. Then using force interpolation functions, the section forces are obtained and subsequently are corrected according to the constitutive law of the fibers. The residual section forces are then multiplied with the section flexibility and integrated along the element length to obtain the element residual deformations. The iterative process at the element level is terminated when the

residual deformations are minimized following an energy convergence criterion. A non-iterative alternative was proposed by Neuenhofer and Filippou (1998).

Force-based elements present localization issues and may lose objectivity at the local or global level, depending on the section constitutive behavior. For elastic-perfectly plastic section responses, the section curvature demands are a function of the number of integration points of the numerical integration scheme used for the integrals. For strain-softening section responses, both the section curvature demands and the element response (and thus the overall structural response) are sensitive to the number of integration points. Strain localization issues also affect displacement-based elements, but the displacement interpolation functions force localization within a single element instead of one integration point (Coleman and Spacone, 2001).

3. Stochastic finite element method

The stochastic finite element method (SFEM) is an extension of the common deterministic process for solving static and dynamic engineering systems, as it involves finite elements with random properties. Stochastic mechanics account for uncertainties in the material properties, geometry of the structure or applied loads, but it is the utilization of the SFEM that allows the derivation and subsequently the evaluation of the stochastic response of the system. The SFEM also arises as a powerful tool for the solution of stochastic (PDEs), from a more mathematical perspective.

A stochastic (or random) field $H(\mathbf{x},\omega)$ is a mapping from a random outcome ω to a function of space (or time) of a random variable x. It is usually called "field" when it varies in space and "process" when it varies in time. The statistical properties of stochastic fields (e.g. probability distribution and correlation structure) are either assumed or obtained from experimental measurements. The general framework of the stochastic finite element method includes the discretization of the stochastic field and the calculation of the response variability (Stefanou 2009).

3.1. Stochastic field discretization

For nonlinear inelastic problems the discretization of the stochastic field requires special attention. As "discretization" we refer to the approximation of the continuous stochastic field $H(\mathbf{x})$ by a finite number of random variables which form a random vector $\hat{H}(\mathbf{x})$:

$$H(\boldsymbol{x}) \xrightarrow{\text{discretization}} \hat{H}(\boldsymbol{x}) = \{H_i\} \tag{8}$$

Common discretization methods are the midpoint method, the integration point method, the local average method, the shape function method and the weighted integral method (Stefanou, 2009). The first two methods are the most popular choices. The midpoint method (Der Kiureghian and Ke, 1988) approximates the stochastic field of every

element Ω_e by a single random variable corresponding to the value of the field at the center x_c of the element, thus:

$$H(\mathbf{x}) \approx \hat{H}(\mathbf{x}_c),\ \mathbf{x}_c \in \Omega_e \tag{9}$$

The approximate field $\hat{H}$ is fully described by the random vector:

$$\mathbf{x} = \{H(x_c^1), H(x_c^2), \ldots, H(x_c^{N_e})\} \tag{10}$$

where N_e is the number of elements of the FE mesh. The mean and the covariance matrix of the field are obtained from the mean, variance and autocorrelation coefficient functions of H evaluated at the center of the element. The integration point method (Matthies *et al*, 1997) differs from the midpoint method since it interpolates the stochastic field at locations that coincide with the integration (or Gauss) points of every element. This scheme is preferred when force-based elements are used.

The choice of the FE mesh size is critical as it affects the discretization of the stochastic field. In principle, the FE mesh size is controlled by the geometry and the expected gradient of the stress field, which in nonlinear problems is not constant during analysis. The discretization of the stochastic field should follow the variation of the field, which is a property of the structure. The variation of the stochastic field is usually measured using the correlation length parameter b, which is the distance over which significant loss of correlation occurs. This quantity determines the degree of correlation between the values $H(x_1)$ and $H(x_2)$ of the stochastic field in two different positions and constitutes a measure of the uncorrelated random variables needed for the field description with satisfactory quality.

In several problems where homogeneous stochastic fields are used, the correlation length is usually defined as:

$$b = \int_0^{\infty} \left|\rho(\tau)\right| d\tau \tag{11}$$

where $\rho(\tau)$ is the normalized (divided by the standard deviation) autocorrelation function of the stochastic field. For example, if:

$$\left|\rho(\tau)\right| = e^{-a|\tau|}, \qquad \alpha>0 \tag{12}$$

the correlation length is given by:

$$b = \int_0^{\infty} e^{-a|\tau|} d\tau = \frac{1}{\alpha} \tag{13}$$

When the correlation length tends to infinity (b→∞), the field is considered as fully correlated. In this case, all the random variables are linearly dependent between them and thus the stochastic field degenerates to a random variable. In the opposite case (b→0), the field tends to the ideal white noise and it is completely uncorrelated.

For all the above reasons, the FE mesh should be dense enough in order to capture the essential features of the random field and avoid loss of information. A recommended element length L_e, suitable for linear displacement-based elements, is given by the formula (Der Kiureghian and Ke, 1988):

$$\frac{b}{4} \le L_e \le \frac{b}{2}. \tag{14}$$

3.2. Calculation of response variability

Different approaches for calculating the response variability of stochastic systems can be found in the literature. The most popular choices are the perturbation approach (based on a Taylor series expansion of the response vector), the spectral method (each response quantity is represented using a series of random Hermite polynomials) and Monte Carlo simulation (MCS). Monte Carlo simulation is the most straightforward and powerful method which entails the generation of a large number of random field realizations and then performing numerical simulations in order to obtain the response quantities of interest. These quantities are then post-processed, to obtain unbiased response estimates and their statistics. The first and the second moment of a response quantity **r** (e.g. displacement, force, stress, etc) can be obtained after *N* simulations as:

$$\begin{aligned} \mu(\mathbf{r}) &= \frac{1}{N}\sum_j^N \mathbf{r}_j \\ \sigma^2(\mathbf{r}) &= \frac{1}{N-1}\left(\sum_j^N \mathbf{r}_j^2 - N\,E^2\left(\mathbf{r}_j^2\right)\right) \end{aligned} \tag{15}$$

A unitless measure of the response variability is also given by the coefficient of variation:

$$COV = \frac{\sigma(\boldsymbol{r})}{\mu(\boldsymbol{r})} \tag{16}$$

With a larger sample size it is possible to estimate the cumulative distribution function (CDF) and the probability density function (PDF) of the response. The direct (crude) MCS is robust, simple to use and has the capability of handling practically every possible problem regardless of its complexity. For that reason, it is often used in the literature as a reference method in order to check the accuracy of other approaches. However the computational cost involved becomes excessive due to the large sample size N required. Hence, it is best to combine MCS with discretization methods that do not involve a large number of random variables (e.g. midpoint method, integration point method). In order to reduce the computational effort, other sampling methods can be used (Hurtado and Barbat, 1998) such as Latin hypercube sampling (LHS), line sampling and subset simulation. Additionally, methods that intend to surrogate the deterministic FEM analysis of every sample realization of the MCS have been implemented in engineering problems, such as the response surface method (RSA – based on statistical regression analysis) and artificial neural networks (ANN – soft computing method based on a heuristic approach) (Papadrakakis et al, 1996).

3.3. Simulation of non-Gaussian stochastic fields

Non-Gaussian stochastic fields are suitable for the description of many practical engineering parameters, such as material properties, geometric characteristics of structural systems, soil properties, waves, wind loads, etc. In order to simulate a non-Gaussian stochastic field, a transformation of a Gaussian field with known second-order statistics must be performed.

The spectral representation method (Shinozuka and Deodatis 1991) is a direct method for the simulation of Gaussian stochastic fields. The method describes the stochastic field as the sum of cosines with random phase angles and amplitudes. It is based on the power spectrum concept, which is a real, non-negative function that describes how the variance of the stochastic field is distributed over the frequency domain. For a one-dimensional univariate (1D-1V) homogeneous Gaussian stochastic field, the *i*-th realization (sample function) is generated from the sum of *M* terms:

$$H^{(i)}(\boldsymbol{x}) = \sqrt{2}\sum_{n=0}^{M-1}\left[A_n \cos\left(\omega_n \boldsymbol{x} + \varphi_n^{(i)}\right)\right] \tag{17}$$

where $\varphi_n^{(i)}$ denotes the random phase angle, which is uniformly distributed in [0,2π] and A_n is the amplitude term, defined as:

$$A_n = \sqrt{2S_{ff}(\omega_n)\Delta\omega} \tag{18}$$

where:

$$\omega_n = n\Delta\omega, \qquad \Delta\omega = \frac{\omega_u}{N} \tag{19}$$

S_{ff} is the power spectral density function of the stochastic field, ω_n is the frequency number (wave number), $\Delta\omega$ is the frequency increment and ω_u the upper-cut frequency after which the power spectrum becomes practically zero. Spectral density functions include the variance and the correlation scale characteristics of the stochastic field and usually are functions of exponential or square exponential type.

The Fourier analysis is fundamental in the application of stochastic fields since all of the properties of a stochastic field can be formulated in a simple and more elegant manner in the space of frequency. In particular, the Fourier transform of the autocorrelation function $R_{ff}(\tau)$ of a homogeneous stochastic field leads to the power spectral density function of this field:

$$S_{ff}(\omega) = \frac{1}{2\pi}\int_{-\infty}^{\infty} R_{ff}(\tau) e^{-i\omega\tau} d\tau \tag{20}$$

The inverse Fourier transform provides the autocorrelation function:

$$R_{ff}(\tau) = \int_{-\infty}^{\infty} S_{ff}(\omega) e^{i\omega\tau} d\omega \tag{21}$$

A power spectrum of square exponential type is shown in Figure 2a for different values of the correlation length *b*, while the influence of the correlation length parameter to the sample functions of a Gaussian stochastic field, generated by the spectral representation method, is shown in Figure 2b.

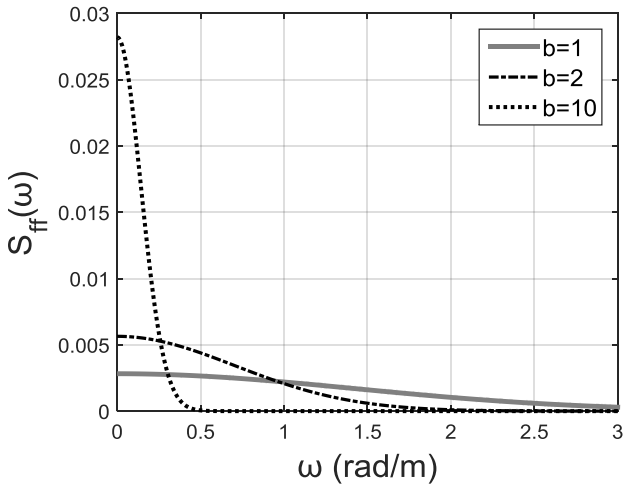

(a)

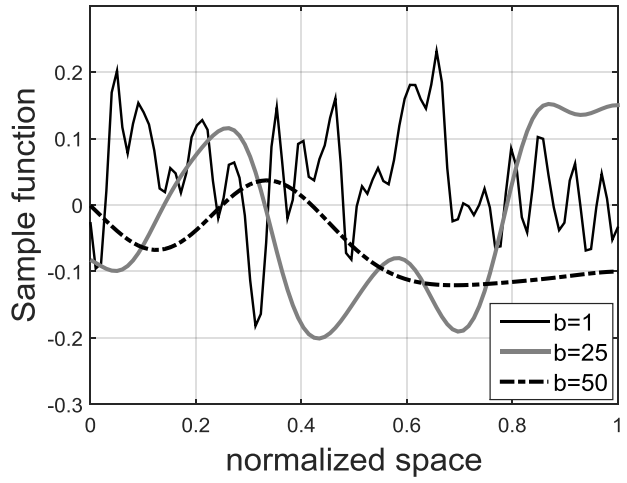

(b)

Figure 2: (a) Sample spectral density function $S_{ff}(\omega)$ of square exponential for different correlation length values (standard deviation, σ_{ff}=0.1), (b) sample functions of a Gaussian stochastic field for different correlation length values *b*.

In order to simulate a non-Gaussian stochastic field, a transformation of a Gaussian field with known second-order statistics needs to be performed. Specifically, a zero-mean homogeneous non-Gaussian stochastic field $f(\mathbf{x})$ with spectral density function $S_{ff}(\omega)$, can be obtained with the aid of a nonlinear monotonic transformation of a zero-mean Gaussian field $H(\mathbf{x})$ as:

$$f\left(\mathbf{x}\right) = F^{-1}\,\Phi\left[H\left(\mathbf{x}\right)\right] \tag{22}$$

where F is the non-Gaussian marginal cumulative distribution function (CDF) of $f(\mathbf{x})$ and Φ is the standard Gaussian CDF. The above transformation is a memoryless

translation of every space coordinate x_i. The choice of the marginal distribution for the translation field $f(\mathbf{x})$ imposes constraints to its correlation structure (Grigoriu 1998). For non-Gaussian translation fields whose autocorrelation function has some inadmissible values, or is not positive-definite, the approximation error should be also taken into consideration (Bocchini and Deodatis 2008, Shields and Deodatis 2013).

4. Proposed methodology

4.1. Theoretical approach

We propose the use of flexibility-based elements for the probabilistic seismic assessment of nonlinear frame structures with stochastic properties. For the deterministic analysis of inelastic frame structures, flexibility-based elements are able to capture the response using a single element per member. When stochastic problems are considered, the frame properties vary along the length of every member. Most FE types require appropriately modifying the FE mesh depending on the properties of the stochastic field and also on the regions where concentration of inelastic demand is expected, i.e. beam ends, region of concentrated forces etc. However, for stochastic problems the critical locations are not known a priori since the structural properties vary. We show that force-based elements, if combined with a pertinent numerical integration scheme, offer accurate estimates of the response variability, maintaining the advantage of a single element per member. The resulting FE scheme is suitable for full-scale frame structures with affordable computing cost and accuracy.

We use stochastic non-Gaussian fields to simulate the material properties. Constitutive laws typically depend on several parameters. For example, a simple bilinear steel model depends on two parameters: the elastic modulus E and the yield stress f_y. More parameters may be required for other material models, e.g. reinforced concrete models. Each material parameter may be denoted as D_i and is distributed along each member following a zero-mean stochastic field $H(\mathbf{x})$. Therefore, if $D_{0,i}$ is the expected value of each parameter, the material property is described as $D_i(\mathbf{x}) = D_{0,i}(1 + H_i(\mathbf{x}))$.

The section stiffness $\mathbf{k}_{\text{sec}}$ is calculated with the aid of Eq. (2), where the constitutive material law is a function of $\mathbf{D} = [D_1, D_2, \ldots, D_N]^T$. For a bilinear steel material $\mathbf{D} = [E, f_y,]^T$ and the section stiffness is obtained as (Eq. (2)):

$$\mathbf{k}_{\text{sec}} = \int_A \mathbf{a}_S^T \frac{\partial \sigma(\mathbf{D})}{\partial \varepsilon} \mathbf{a}_S^T dA \tag{23}$$

The element stiffness matrix is calculated with Gauss-Lobatto quadrature, as:

$$\begin{aligned} &\mathbf{K}_N = \int_L \mathbf{b}^T \mathbf{k}_{\text{sec}}^{-1} \mathbf{b}^T dL \Leftrightarrow \\ &\mathbf{K}_N = w_1 \mathbf{b}^T(x_1)\mathbf{k}_{\text{sec}}^{-1}(x_1)\mathbf{b}(x_1) + w_{NIP}\mathbf{b}^T(x_{NIP})\mathbf{k}_{\text{sec}}^{-1}(x_{NIP})\mathbf{b}(x_{NIP}) + \\ &+ \sum_{i=2}^{NIP-1} w_i \mathbf{b}^T(x_i)\mathbf{k}_{\text{sec}}^{-1}(x_i)\mathbf{b}(x_i) \end{aligned} \tag{24}$$

where *NIP* is the number of integration points, w_i and x_i are the weights and the location of Gauss-Lobatto integration sections. Note that x_1 and x_{NIP} refer to the two ends of the beam element. This integration scheme is also adopted for the element internal forces. The above methodology is implemented with the aid of OpenSees (McKenna and Fenves 2001). OpenSees is an open-source structural analysis software that allows the user to define any numerical integration scheme. The pre and the post processing of our results are performed with the aid of customized in-house software.

We first generate zero-mean Gaussian stochastic fields using the spectral representation method (Eq. (17)). These fields have a spectral density function of square exponential type:

$$S_{HH}(\omega) = \frac{\sigma^2 b}{2\sqrt{\pi}} \exp\left(-\frac{b^2\omega^2}{4}\right) \tag{25}$$

where σ is the standard deviation of the stochastic field and b is the correlation length parameter. The lognormal fields are subsequently obtained using Eq. (22).

The required number of integration points strongly depends on the correlation length b of the stochastic field. Figure 3a and 3b show two stochastic fields with correlation lengths equal to 10 and 100, respectively. Both fields are integrated using five Gauss-Lobatto integration points. For the small correlation length (b=10, Figure 3a) the number of integration points is not adequate, while as the correlation length increases

the five integration points are able to sufficiently capture the variation of the properties along the beam's length.

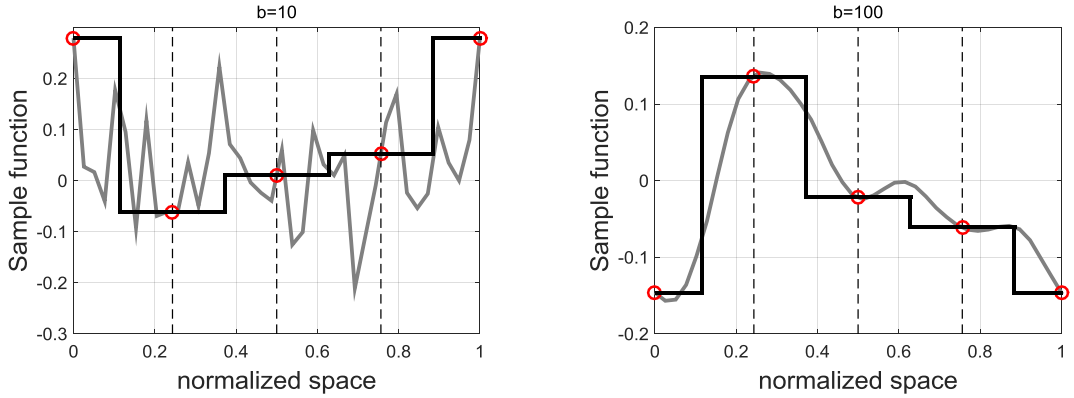

(a) (b)

Figure 3: Stochastic field description using five integration points: (a) b=10, small correlation length: the number of integration points is not sufficient causing loss of information, and (b) b=100, large correlation length: the five integration points are enough.

In the remainder of the paper we consider as reference, or "correct", solution, FE models that use a very dense mesh of 50 displacement-based fiber elements per member. Such a dense mesh is expected to accurately describe randomness for any correlation length. In the latter case, due to the short length of the displacement-based elements, the stochastic field is interpolated using the midpoint method.

4.2. Computational implementation

We use MATLAB (2014) for the implementation of the spectral representation method and the consequent generation of the lognormal stochastic fields (see Appendix C). The stochastic mesh is quite dense for a qualitative description of the continuous fields, since it is required only once throughout the Monte Carlo simulations. The appropriate fields' values corresponding to the Gauss-Lobatto integration points are stored in data files, to be processed later by OpenSees. The number of integration points is essentially the finite element mesh of the method. If we assume a force-based beam element with 20 integration points, a temporary OpenSees file with the form of Figure 4 must be exported from MATLAB for each Monte Carlo realization. The variables f and g represent the first and second stochastic field respectively, assuming steel material with two random parameters (E and f_y).

```
set f1 0.197391
set g1 -0.058184
set f2 0.325228
set g2 -0.140837
set f3 -0.023358
set g3 -0.081030
.
.
.
set f20 0.197391
set g20 -0.058184
```

Figure 4: Stochastic field values of temporary OpenSees file

The main OpenSees file reads the temporary file (Stoch_field.tcl) for each realization and sets the stochastic field values into lists, in order to propagate them into the Gauss-Lobatto integration of the element. An example of the implementation of the values to the material properties according to equation $D_i(\mathbf{x}) = D_{0,i}(1 + H_i(\mathbf{x}))$, is presented in Figure 5.

After setting the material properties, the 20 different material tags must be assigned to the 20 Gauss points of the force-based element. This is done by creating 20 sections, each one corresponding to the material tags and subsequently using these sections for the integration input. We choose the "User-defined integration" out of the many force-based integration options of OpenSees, simply because it allows total freedom to the user regarding locations and weights but most importantly because it does not have limitations regarding the number of integration points. With the user-defined integration option the user can easily switch to other numerical integration schemes (Gauss-Radau, Newton-Cotes etc.).

After setting the integration input, the beam element input is straightforward. The important thing is the consistency of the main OpenSees file, so that the stochastic field values of the integration points are updated in each Monte Carlo realization, simply by sourcing the updated temporary OpenSees file of the new values. The integration propagation process mentioned above is presented in Figure 6. It is noted that the values of locations and weights of the Gauss-Lobatto integration points, can be sourced from a

file generated by MATLAB (see Appendix B) in order to avoid stating all these values by hand.

```
source Stoch_field.tcl

# Steel attributes – mean values (kN/m^2)
set fy 235e3;
set E 210e6;

set f [list $f1 $f2 $f3 $f4 $f5 $f6 $f7 $f8 $f9 $f10 \
          $f11 $f12 $f13 $f14 $f15 $f16 $f17 $f18 $f19 $f20]
set g [list $g1 $g2 $g3 $g4 $g5 $g6 $g7 $g8 $g9 $g10 \
           $g11 $g12 $g13 $g14 $g15 $g16 $g17 $g18 $g19 $g20]

for {set i 1} {$i <=20} {incr i} {
        set a [lindex $f $i-1]
        set b [lindex $g $i-1]
        lappend Elist [expr $E*(1+$a)]
        lappend fylist [expr $fy*(1+$b)]
}

# Bilinear material (S_235) law with hardening
# uniaxialMaterial Steel01 $matTag $Fy $E0 $b <$a1 $a2 $a3 $a4>

for {set i 1} {$i <=20} {incr i} {
        set a [lindex $Elist $i-1]
        set b [lindex $fylist $i-1]
        uniaxialMaterial Steel01 $i $b $a 0.000001
}
```

Figure 5: Code for the propagation of the stochastic fields in the material properties

```
for {set i 1} {$i <=20} {incr i} {
        lappend sectag $i
}

# HEB 200
for {set i 1} {$i<=20} {incr i} {
        set a [lindex $sectag $i-1]
        # section WFSection2d $secTag $matTag $d $tw $bf $tf $Nfw $Nff
        section WFSection2d         $a         $i     0.2  0.009  0.2  0.015 15  5
}

#Gauss - Lobatto Integration
set locations "0   0.009628147553043   0.032032750593667   0.066561010955025  \
0.112315869523972   0.168111798854844   0.232503567984057  \
0.303823408143045   0.380224147038507   0.459727031380589  \
0.540272968619411   0.619775852961493   0.696176591856955  \
0.767496432015943   0.831888201145156   0.887684130476028  \
0.933438989044975   0.967967249406333    0.990371852446957   1.0"

set weights "0.002631578947368   0.016118561594244   0.028590901063783  \
0.040315881998060   0.050995749849725   0.060354613814337  \
0.068150241179362   0.074180777035458   0.078290051323738  \
0.080371643193923   0.080371643193923   0.078290051323738  \
0.074180777035458   0.068150241179362   0.060354613814337  \
0.050995749849725   0.040315881998060   0.028590901063783  \
0.016118561594244   0.002631578947368"

set sectags "1 2 3 4 5 6 7 8 9 10 11 12 13 14 15 16 17 18 19 20";

set np 20;
set integration "UserDefined $np $sectags $locations $weights";

geomTransf Corotational 2;    # all geometric nonlinearities

# element forceBeamColumn $eleTag $iNode $jNode $transfTag "IntegrationType"
element forceBeamColumn         1         1         2         2         $integration
```

Figure 6: Code for the propagation of stochastic fields in the element integration

5. Steel portal frame example

We first consider as a case study the steel portal frame of Figure 7. All the members of the frame have HEB 200 wide flange cross-sections and are modeled with a single force-based beam-column element. A distributed load q=40kN/m is applied at the bay and remains constant throughout the loading history. The uncertain material properties are the Young's modulus E and the yield stress f_y, both assumed to vary stochastically along each member according to the two fields H_1 and H_2. Therefore, the material properties are described by the expressions:

$$\begin{aligned} E(x) &= E_0\left[1+H_1(x)\right] \\ f_y(x) &= f_{y0}\left[1+H_2(x)\right] \end{aligned} \tag{26}$$

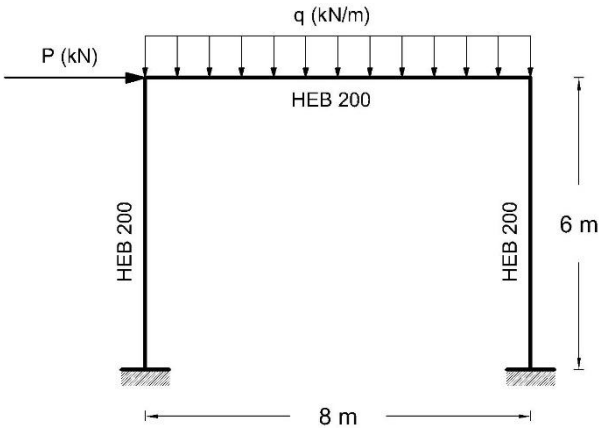

Figure 7: One-storey steel frame.

where $H_1(\mathbf{x})$, $H_2(\mathbf{x})$ are two zero-mean 1D-1V homogeneous lognormal stochastic fields. The COV for both fields was assumed equal to 10% as indicated by the Joint Committee for Structural Safety (JCSS, 2001). Different values of the correlation length parameter b are considered in order to investigate the sensitivity of the response to the correlation scale of the fields.

5.1. Nonlinear static analysis

Nonlinear static analysis is a valuable tool for the seismic capacity assessment of frame structures. The response variability of the steel portal frame is calculated for a sample size of 500 crude Monte Carlo simulations. For every simulation we obtain the capacity curve in terms of drift versus applied load. The mean capacity curve of the frame is shown in Figure 8, together with the mean plus and the mean minus one standard deviation curves. The vertical dashed line separates the pre-yielding from the post-yielding phase of loading. Figure 8a clearly shows that the effect of the elastic modulus is rather small (pre-yielding phase), while considerable variability is observed after yielding where f_y comes into play (right of the dashed line).

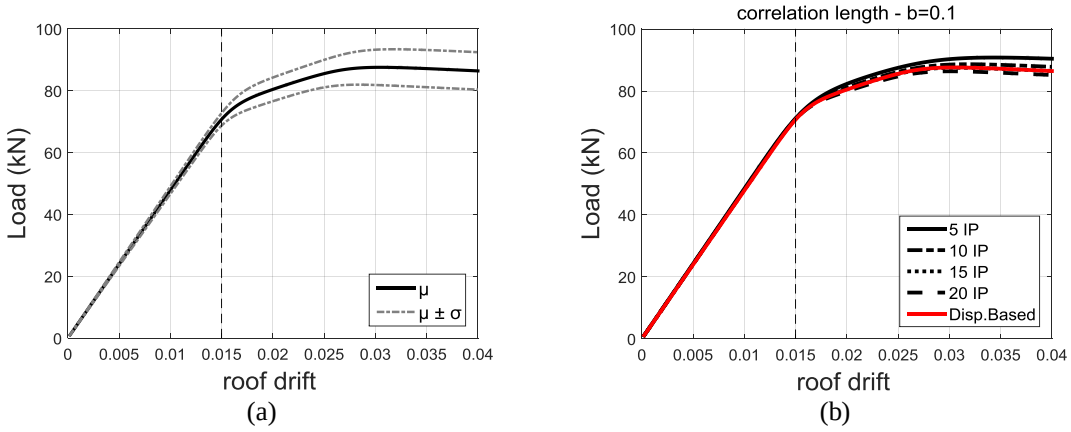

Figure 8: (a) Mean and mean ± one sigma capacity curves of the portal frame, (b) mean capacity curves for ranging number of integration points.

According to Figure 8b the calculation of the mean capacity is not sensitive to the number of integration sections even for this small correlation length (b=0.1). On the other hand, Figure 9 examines the necessary number of integration points in order to capture the response variability defined as the COV conditional on the drift. As reference solution we use the red solid curve obtained with the aid of a very dense mesh of 50 displacement-based elements per member. For four correlation length values, we compare the COV estimates using force-based elements of 5, 10, 15 and 20 integration sections. All four plots of Figure 9 show that increasing the number of integration points the COV values converge to the "correct" solution. This means that more integration points offer a better description of the random fields. The convergence is faster as the

correlation length *b* becomes large, e.g. compare Figure 9a and Figure 9d. The vertical dashed line (defined in Figure 8) provides the threshold between linear elastic and inelastic response. In the elastic region, the COV is practically constant and very low, of the order 2-6%. When the frame starts to yield, the COV increases almost monotonically as the drift also increases.

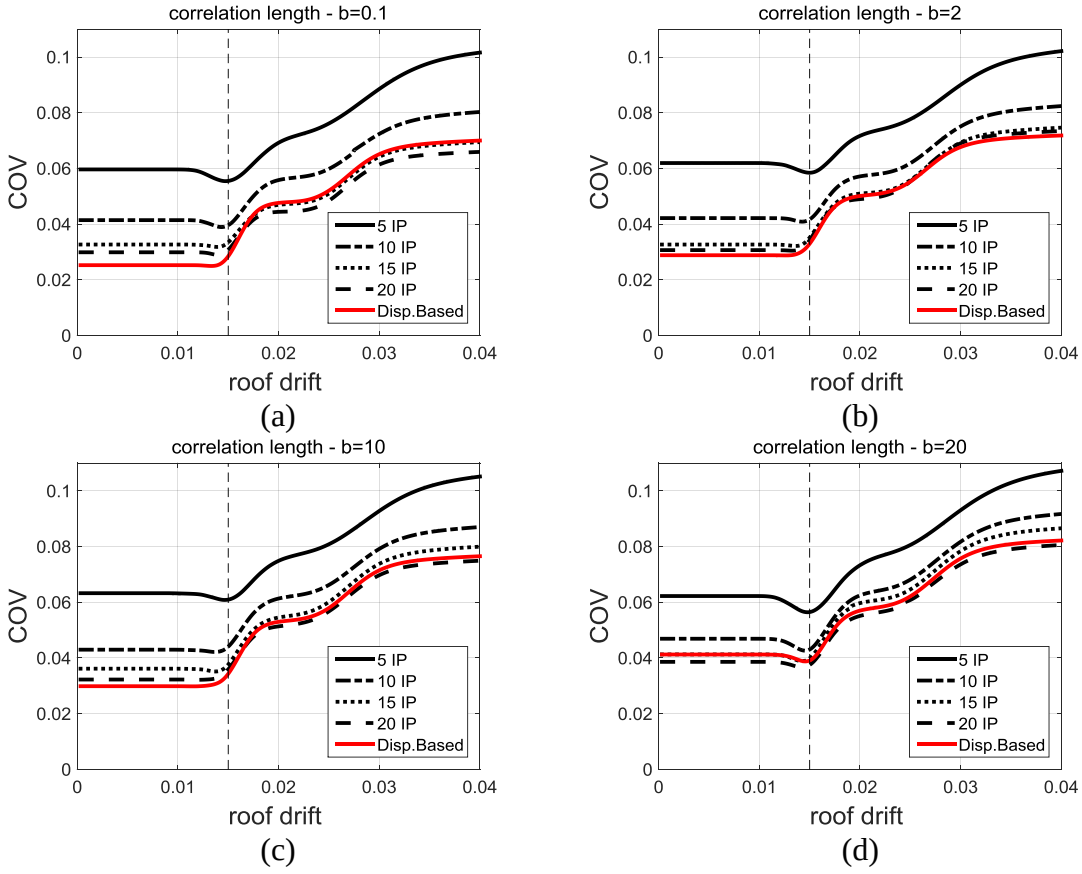

Figure 9: Sensitivity of response variability to the number of integration points for different correlation lengths: (a) *b*=0.1, (*b*) *b*=2, (*c*) *b*=10 and (*d*) *b*=20.

The accurate modelling should account for the correlation scale and hence the variance of the field through its power spectrum. According to Figure 9, the simulation without the proper number of integration sections is insensitive to the spectral characteristics of the stochastic fields (e.g. Figure 9, five integration sections). This is also verified in Figure 10 where we study the effect of the correlation length *b* comparing the variation of the "correct" solution shown (Figure 10a), to that of a force-based element with 5 integration sections (Figure 10b). Since five integration sections

are not adequate, all curves of Figure 10b practically coincide and thus are unable to predict the response variation accurately.

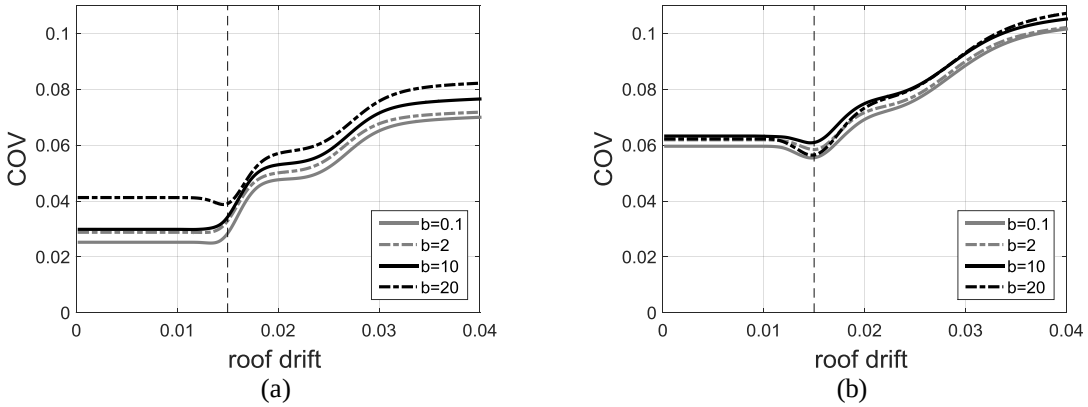

Figure 10: Correlation length sensitivity: (a) "correct" solution and (b) poor description offered from a mesh of force-based elements with 5 integration points.

As mentioned in Chapter 2, force-based elements often suffer from localization effects and may lose objectivity in local or global scale. Loss of objectivity means that a possible increase of integrations points does not lead to a convergence of the results. Perfectly plastic and softening sectional responses are the most susceptible to non-objective responses (Coleman and Spacone, 2001).

The deformation localization due to the numerical integration of the element integrals is typically observed at the end integration points, where the bending moments reach their maximum value. This is verified by the portal frame example as shown in Figure 11, where the curvatures of the left column's lowest integration sections developed during the static analysis, have been plotted against the incremental horizontal load for the deterministic problem (the IP 1 is the integration point closest to the fixed end). However, for the stochastic problem due to the material properties variance irregularities may occur, as in Figure 12, where localization occurs at the third integration point, for a single realization of the stochastic fields.

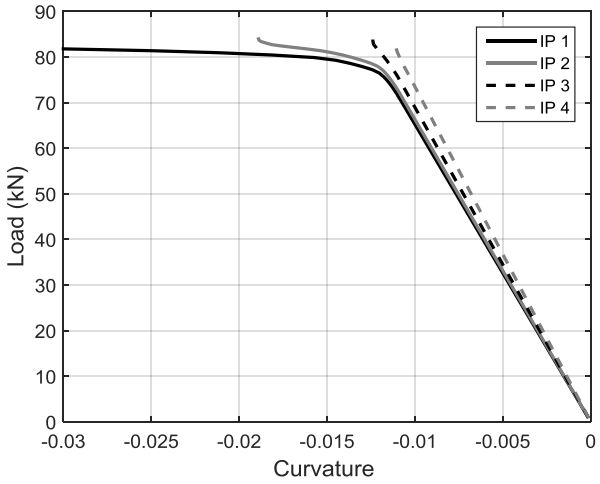

Figure 11: Curvatures against load for the deterministic problem.

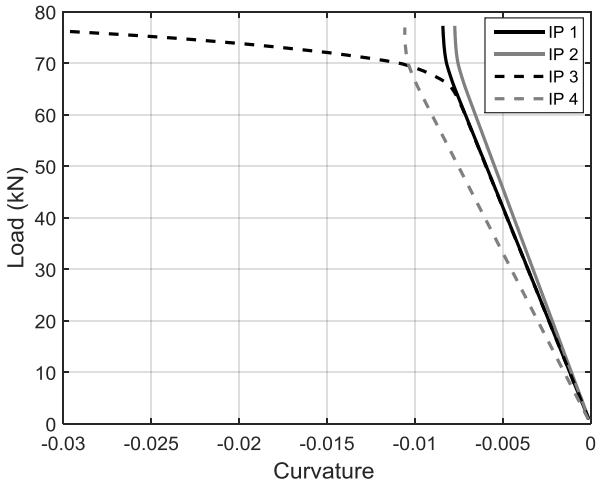

Figure 12: Curvatures against load for the stochastic problem.

The aforementioned are more obvious as presented in Figure 13, where the curvature distribution along the column height is plotted for a pre-yield and a post-yield snapshot, for all 20 Gauss-Lobatto integrations sections. The stochastic variation and the interaction of stiffness and strength variability cause irregularities to the curvature distribution (Figure 13b). Nevertheless, these irregularities of the individual stochastic realizations are not mirrored on the mean curvature distribution, as it can be shown in Figure 14, where the curvature distribution of the ensemble average is again smooth.

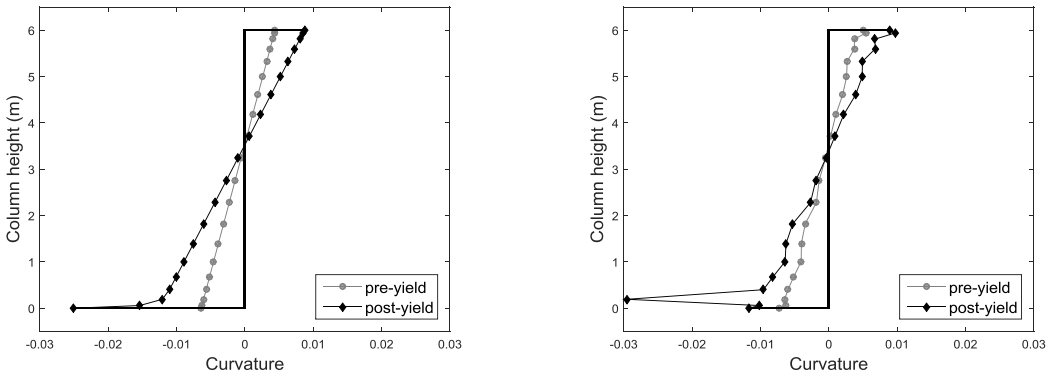

Figure 13: Curvature distributions for: (a) the deterministic problem and (b) the stochastic problem

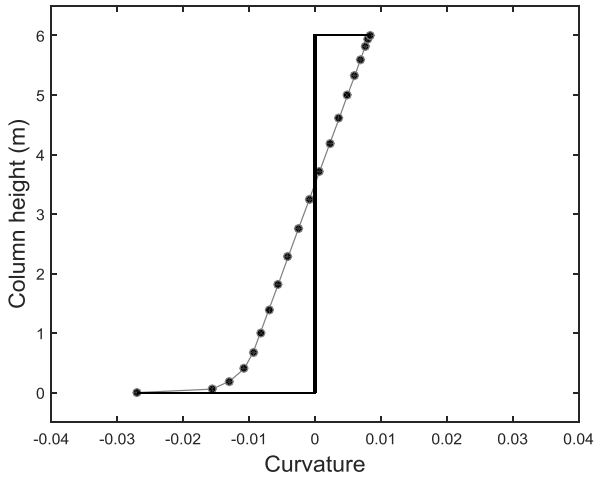

Figure 14: Mean curvature distribution (stochastic ensemble average)

For the above example, no loss of objectivity is observed on the response, in terms of capacity curves. In Figure 15a we present the deterministic capacity curves for different numbers of integration points and in Figure 15b the capacity curves for different stochastic fields are presented. It is clear that in the second case the variability is exclusively because of the stochastic variability, as it is in terms of pure translation (the path shape in every case is the same).

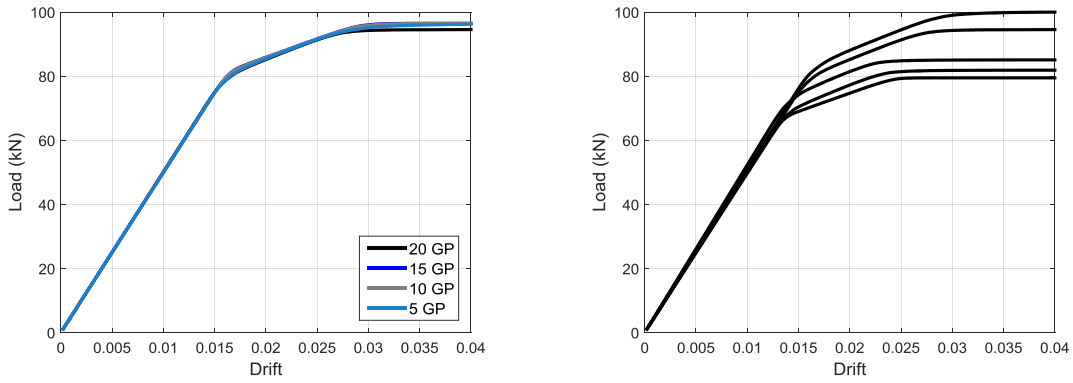

Figure 15: (a) Deterministic capacity curves with respect to the number of integration points (b) capacity curves for different stochastic fields

5.2. Nonlinear response history analysis

The seismic performance of the steel portal frame is also studied using nonlinear response history analysis. Nonlinear response history analysis using ground motion records is considered the most realistic and accurate analysis method available (Fragiadakis *et al.* 2014). Seismic demand is measured with the aid of the maximum drift ratio (θ_{max}). A lumped mass matrix is formed in agreement to the distributed load q (Figure 7), while the fundamental mode of the frame was found equal to T_1=1.24sec when the mean value of the Young modulus E is used. The damping matrix was obtained assuming 5%-Rayleigh damping on the first and the second mode. All response history analyses were performed using for every member a single force-based beam-column element with 20 Gauss-Lobatto integration sections. Again we assume that the "correct" solution is that of a dense mesh of displacement-based elements.

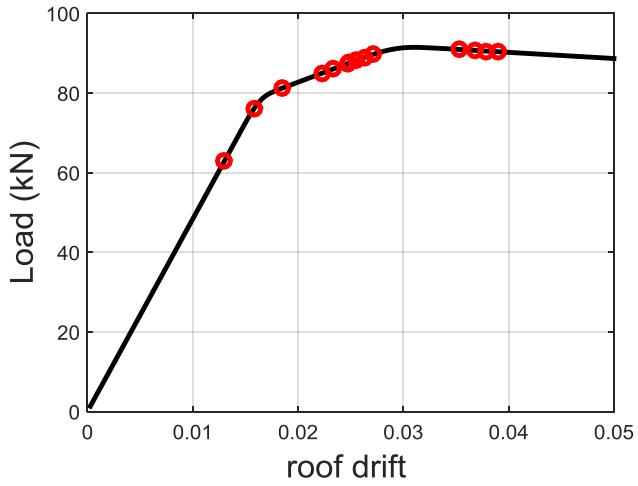

Figure 16: Drift demand of the natural ground motion records of Table 1 (red circles) plotted on the capacity curve of the frame (solid line).

All response history analyses are performed with the fifteen ground motion records of Table 1. The records cover a wide range of seismic intensities in order to evaluate the structural behavior at different levels of seismic demand. All records are scaled with a uniform scaling factor equal to 2. This guarantees that some of the records will yield the frame. Figure 16 shows the maximum drift demand for every record plotted against the capacity curve of the frame. The drift values were obtained with assuming mean values for the random variables. The response practically convergences after 300 Monte Carlo simulations, regardless of the correlation scale. This is shown in Figure 17 where the evolution of the first two statistical moments of storey drift for two different values of the correlation length parameter (b=0.1 and b=10) are computed for the Loma Prieta 1989 (WAHO) record (Table 1).

Table 1: Natural ground motion records considered

No.	Event	Station	φ°*	Soil†	M‡	R§(km)	PGA(g)
1	Imperial Valley, 1979	Compuertas	015	C,D	6.5	32.6	0.186
2	Loma Prieta, 1989	Agnews State Hospital	090	C,D	6.9	28.2	0.159
3	Loma Prieta, 1989	Anderson Dam Downstrm	360	B,D	6.9	21.4	0.24
4	Loma Prieta, 1989	Halls Valley	090	C,C	6.9	31.6	0.103
5	Loma Prieta, 1989	Coyote Lake Dam Downstrm	285	B,D	6.9	22.3	0.179
6	Loma Prieta, 1989	WAHO	000	-,D	6.9	16.9	0.37
7	San Fernando, 1971	LA, Hollywood Stor. Lot	090	C,D	6.6	21.2	0.21
8	Superstition Hills, 1987	Wildlife Liquefaction Array	090	C,D	6.7	24.4	0.18
9	Loma Prieta, 1989	Hollister Diff. Array	255	-,D	6.9	25.8	0.279
10	Loma Prieta, 1989	Hollister Diff. Array	165	-,D	6.9	25.8	0.269
11	Loma Prieta, 1989	Sunnyvale Colton Ave	270	C,D	6.9	28.8	0.207
12	Imperial Valley, 1979	Chihuahua	282	C,D	6.5	28.7	0.254
13	Loma Prieta, 1989	Sunnyvale Colton Ave	360	C,D	6.9	28.8	0.209
14	Loma Prieta, 1989	WAHO	090	-,D	6.9	16.9	0.638
15	Superstition Hills, 1987	Wildlife Liquefaction Array	360	C,D	6.7	24.4	0.2

* Component
† USGC, Geomatrix soil class
‡ Moment Magnitude
§ Closest distance to fault rupture

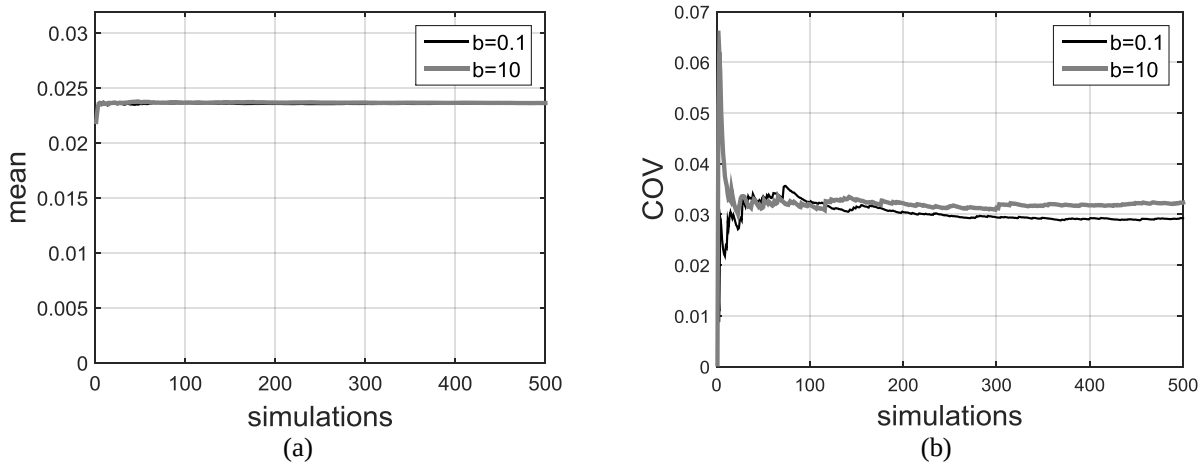

(a) (b)

Figure 17: Statistical convergence of (a) mean and (b) COV of drift for *b*=0.1 and *b*=10 (record: *Loma Prieta 1989, WAHO*)

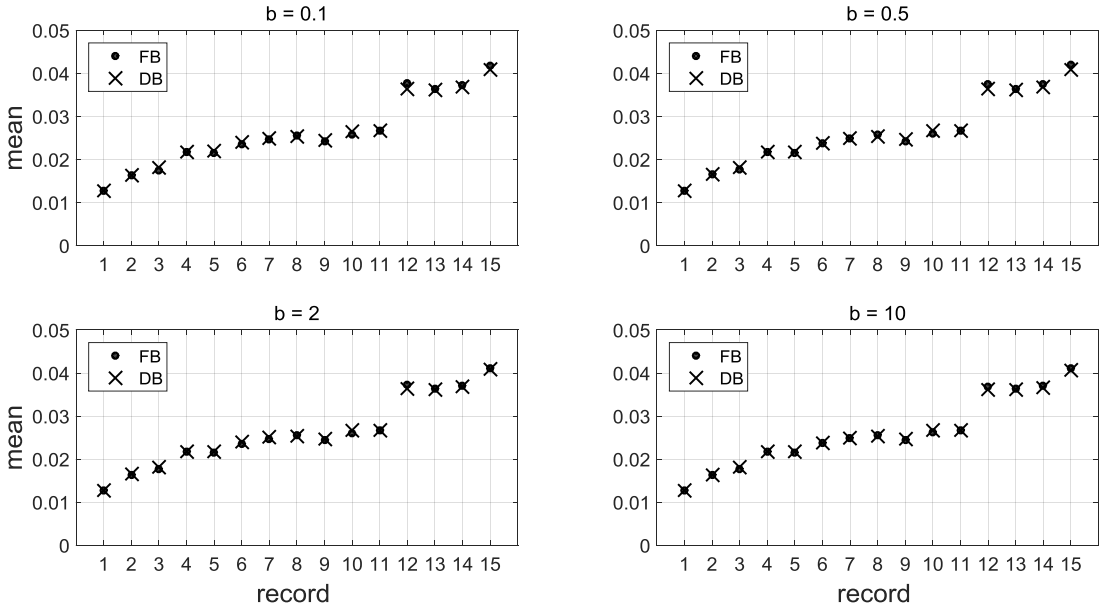

Figure 18: Mean drift demand for correlation values equal to b=0.1, 0.5, 2 and 10.

The accuracy of the proposed method is examined considering the first three statistical moments and the sensitivity of the drift θ_{max} with respect to the correlation length and the ground motion record considered. Figure 18 shows the mean storey drift (θ_{max}) for four values of the correlation length, i.e. b = 0.1, 0.5, 2 and 10. The proposed force-based modeling provides results that are practically identical to the "correct" solution. Note that in Figure 18, the records are sorted from left to right according to the maximum expected drift demand (Figure 16).

Figure 19 shows the effect of stochastic material properties on the COV of drift (θ_{max}) demand. For all b values considered, the accuracy of the force-based formulation is again very close to the correct solution. The errors observed are small proving that the discretization with 20 sections is sufficient. Furthermore, records that do not cause large inelastic demand (records towards the left) have smaller COV values than records that caused inelastic damage on the building (records towards the right). Still, the COV values are very sensitive to the record characteristics while, for most ground motions, the COV of the response is lower than the variance of the stochastic input parameters. In Figure 20 we group the COV values for every record for different correlation length values. The effect of the correlation length is small compared to the significance of the ground motion properties, while large correlation lengths tend to increase the COV.

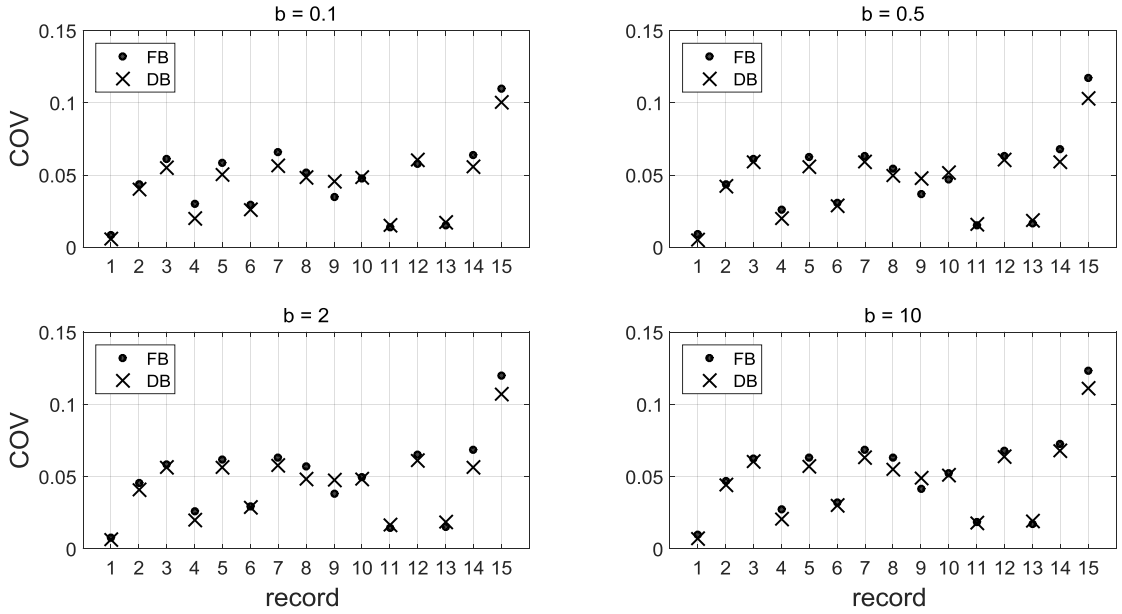

Figure 19: COV of drift demand for correlation values equal to *b*=0.1, 0.5, 2 and 10.

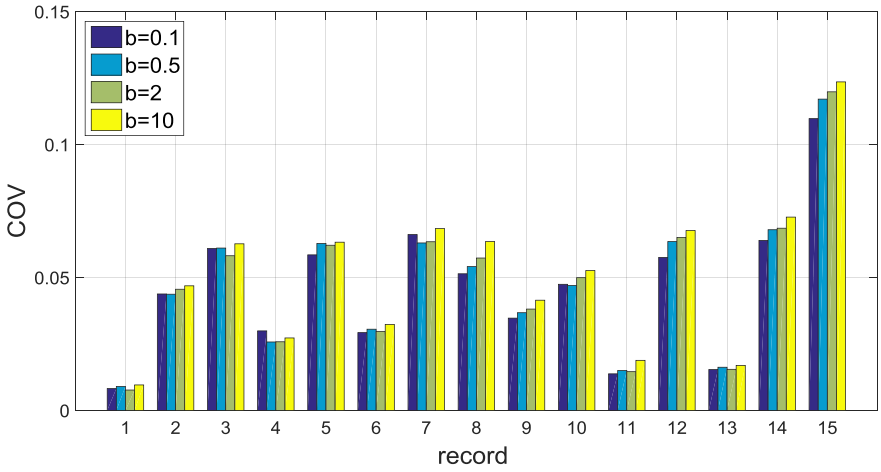

Figure 20: COV of maximum storey drift with respect to the correlation length parameter *b*.

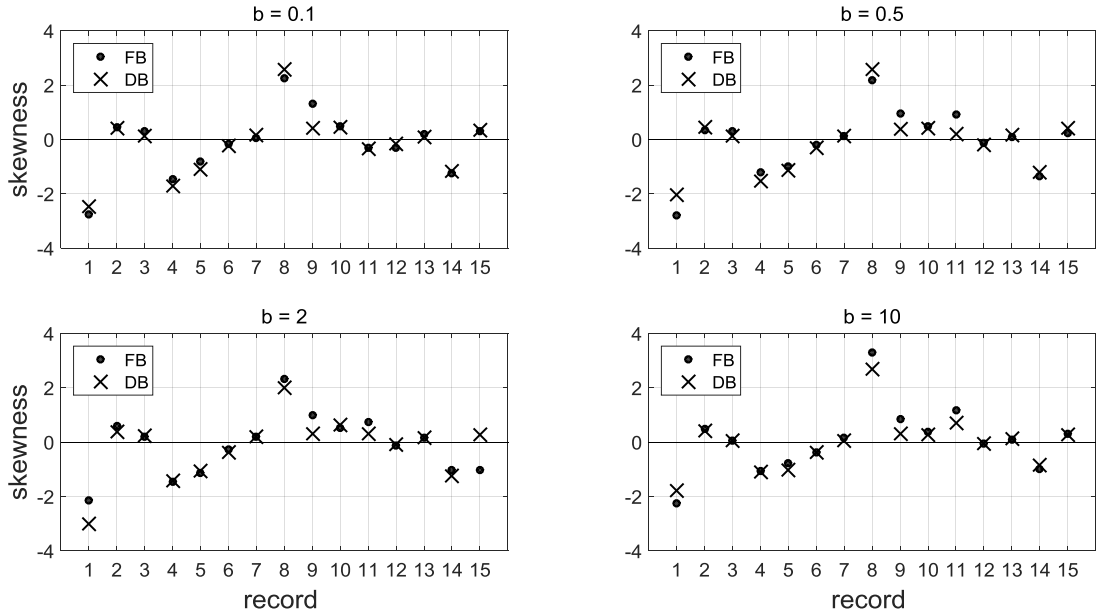

Figure 21: Skewness of drift demand for correlation values equal to *b*=0.1, 0.5, 2 and 10.

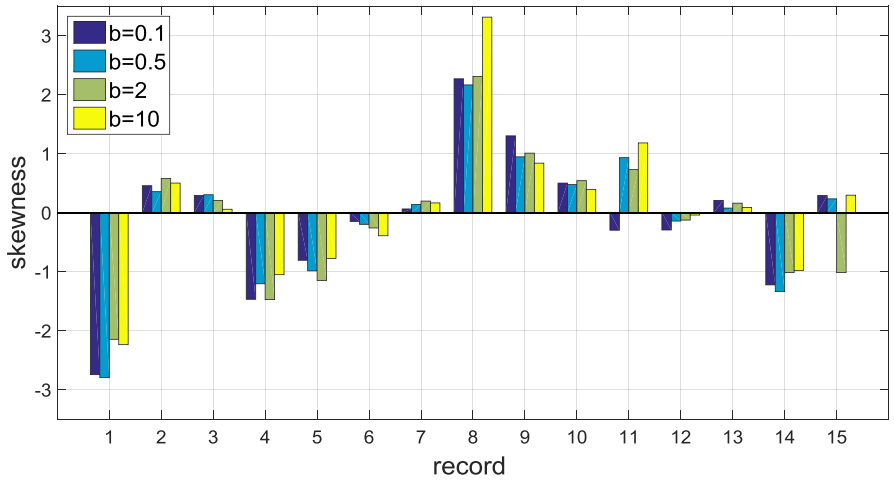

Figure 22: Skewness of maximum storey drift demand with respect to the correlation length parameter *b*.

Figure 21 and Figure 22 show the skewness (third statistical moment). The skewness provides a measure of the asymmetry of sample's probability density function. Figure 22 shows the skewness as function of the correlation length *b*. Contrary to the COV case, the skewness is quite sensitive to the correlation length and varies with the record properties. For many records the skewness differs considerably for different *b* values and doesn't follow the properties of the lognormal material/input properties.

Furthermore, samples of opposite skewness for the same natural record, e.g. records 11 and 15, were found. In all cases, the proposed modeling gave excellent estimates of the skewness when compared to the correct solution and despite the inherent sensitivity of the problem to this parameter (Figure 21).

The effect of record-to-record variability is further examined looking at the probability density function (PDF) of the maximum storey drift demand. The PDF is calculated with the aid of the kernel density estimation method (Bowman and Azzalini, 1997). Figure 23a compares the PDFs of a randomly chosen ground motion for different correlation length values. The sensitivity of the shape of the PDF with respect to the correlation length is rather small but cannot be overlooked. However, if we examine the PDFs of different ground motions and assume the same correlation length (e.g. b=0.1), the PDFs differ considerably in terms of both COV and skewness (Figure 23b). Still, however, all PDFs are unimodal and retain the lognormal PDF shape of the input variables.

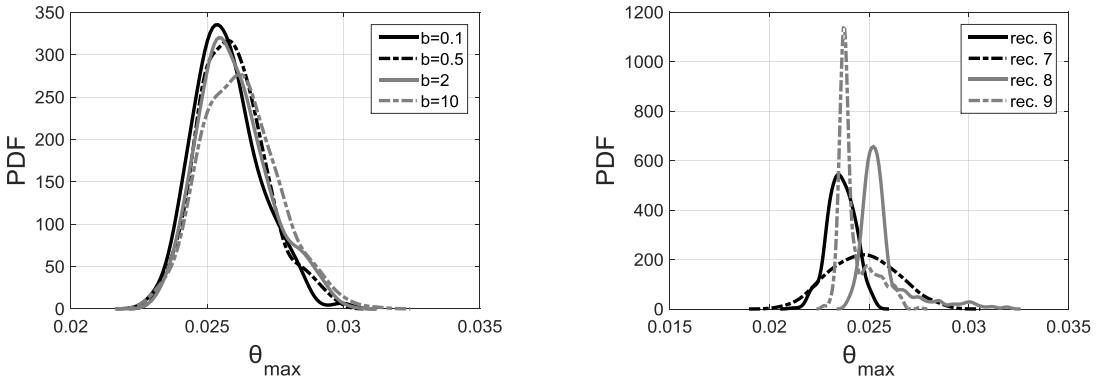

Figure 23: Response probability density functions: (a) effect of correlation length (record: *Loma Prieta 1989, Sunny Colton Ave*), (b) effect of different ground motion records (b=0.1, constant).

Apart from accuracy, the proposed method also reduces considerably the computing cost. Figure 24 compares the computational cost of the proposed element to that of the displacement-based formulation for both static and dynamic analysis. An Intel Core 2 Duo processor required more than double time to run 500 Monte Carlo simulations for the nonlinear static case. For the stochastic response history analysis with a single record (Superstition Hills, 1987), the proposed methodology required approximately 10% of the time of the displacement-based element for the same number of simulations.

Although the computational effort of the displacement-based element can be reduced using a more coarse mesh, Figure 24 provides a clear indication of the exceptional computing performance of the force-based element which can be adopted for the simulation of real-scale problems.

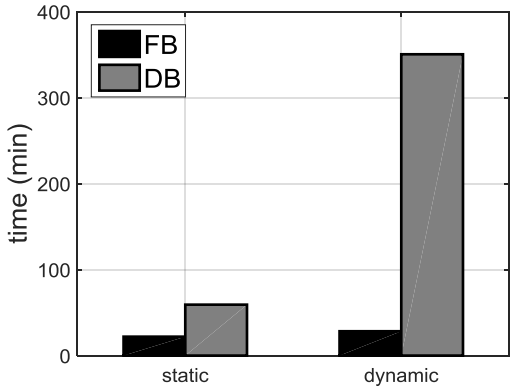

Figure 24: Computing cost of 500 Monte Carlo simulations of the portal frame for the force-based and the displacement-based formulation.

6. Reliability assessment of a reinforced concrete bridge

6.1. Model description

The second case-study is a reinforced concrete bridge inspired from the Arahthos-Peristeri Bridge in Egnatia Highway (Figure 25). The bridge model has a total length of 240m and is shown in Figure 26. The slab of the deck is continuous and is assumed monolithically connected to the piers. Our finite element model assumes that the abutments are free to move in the longitudinal direction, while the piers are assumed fully fixed. The deck has a box-girder cross-section (Figure 27a) and 13.5m total width. The piers are wall-like columns and their cross-section is rounded, as shown in Figure 27b.

Figure 25: Arahthos-Peristeri Bridge in Egnatia Highway

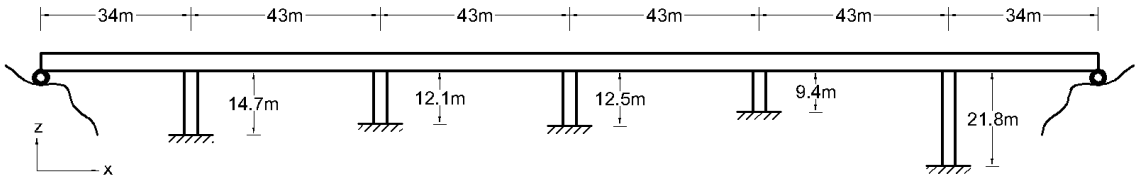

Figure 26: Bridge model.

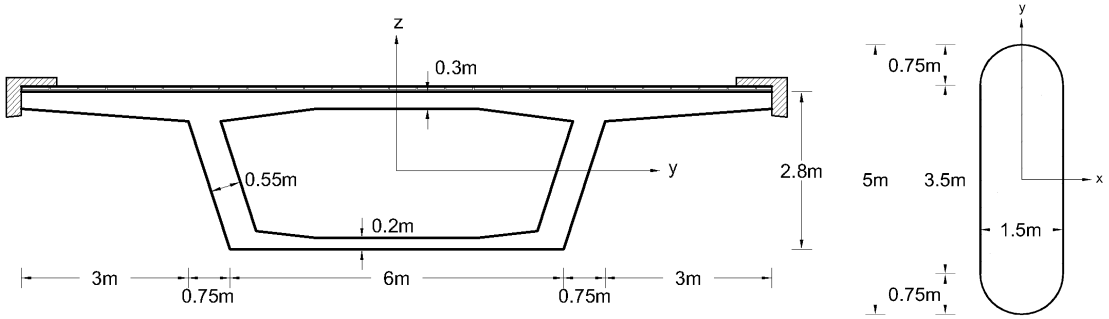

(a) (b)

Figure 27: Cross-sections of: (a) deck and (b) bridge piers.

The reinforced concrete sections of the piers are discretized assuming unconfined concrete properties for the cover and confined properties for the core. Both cover and core were modelled with a uniaxial Kent-Scott-Park concrete material model (McKenna and Fenves, 2001) with degraded linear unloading/reloading stiffness. The tensile strength of concrete is neglected for both the confined and the unconfined case. Furthermore, a bilinear law with pure kinematic hardening is assumed for the reinforcing steel fibers. Three parameters were chosen to vary along the members following uncorrelated lognormal stochastic fields: the compressive strength f_c, the corresponding strain ε_c and the steel yield stress f_y of the reinforcement. The same stochastic field was used for the confined and the unconfined concrete of every cross section. The mean values and the COV of the lognormal stochastic fields are shown in Table 2. The COV values assumed were obtained from JCSS (2001) and are in agreement with typical values in the literature which are summarized in Dymiotis *et al.* (1999). Three different stochastic fields are produced, denoted in Table 2 as H_1, H_2 and H_3. The stochastic field that each random parameter follows is shown in the last column of Table 2.

Table 2: Properties of the RC cross-sections of the piers

Random parameter	mean	COV	stochastic field
Compressive strength (confined)	45MPa	20%	H_1
Compressive strength (unconfined)	27.6MPa	20%	H_1
Ultimate strength (confined)	44MPa	20%	H_1
Ultimate strength (unconfined)	0MPa	20%	H_1
Compressive strain (confined)	3.67‰	20%	H_2
Compressive strain (unconfined)	2‰	20%	H_2
Crushing strain (confined)	36‰	20%	H_2
Crushing strain (unconfined)	6‰	20%	H_2
Reinforcement yield stress	460MPa	10%	H_3

The bridge piers are simulated with a single force-based fiber beam-column element assuming 20 Gauss-Lobatto integration sections per member. The deck is simulated with elastic beam elements, while appropriate restraints were imposed in order to ensure its rigid diaphragm behavior. Moreover, a uniformly distributed load of 300kN/m is applied on the bridge deck in order to simulate the loads on the bridge. The response of the bridge is dominated by the first mode which corresponds to an eigenperiod equal to T_1=0.342sec for the mean values of all parameters. The damping matrix is formed proportional to the mass and the stiffness (Rayleigh damping) assuming 5% damping for the first two modes.

6.2. Fragility assessment

Seismic fragility is defined as the probability that a structural system violates a limit-state when subjected to an earthquake of given intensity. The seismic intensity is measured with the aid of an intensity measure. A commonly adopted intensity measure is the 5%-damped first-mode spectral acceleration $S_a(T_1,5\%)$. Therefore, the limit-state fragility curve is expressed as:

$$F_R(x) = P\left[LS_i \left| S_a\left(T_1, 5\%\right) = x \right. \right] \tag{27}$$

where LS_i represents the exceedance of the i^{th} limit-state. A limit-state is exceeded when the demand exceeds the corresponding limit-state capacity, both measured with the aid of an engineering demand parameter (EDP). The EDP adopted for the bridge problem is the maximum drift $\theta_{\max}$ of the shortest pier.

We use the Monte Carlo simulation method in order to calculate Eq. (27) for increasing levels of the intensity measure. We therefore scale the ground motion records of Table 1 and subsequently calculate Eq. (27) as the conditional probability that $\theta_{\max}$ exceeds the limit-state capacity $\overline{\theta}_{\max}$. The limit-state probability is calculated from the empirical distribution, simply as:

$$P_{LS} \cong \frac{N_H}{N_{sim}} \tag{28}$$

where N_H is the number the simulations where θ_{max} exceeds the threshold/capacity drift for the limit-state examined, and N_{sim} is the total number of simulations per intensity level.

The fragility curves are calculated for three different cases: (i) lognormal stochastic fields with b=0.2, (ii) lognormal stochastic fields with b=10 and (iii) the random parameters are considered lognormal random variables, which practically is equivalent to a stochastic field with very large correlation length. The latter assumption is very common in earthquake engineering applications. Figure 28 shows the fragility curves for three limit-states, i.e. $\overline{\theta}_{\max} \geq$ 0.25%, 0.5% and 1%. As shown in Figure 28, the assumption of modelling the frame properties as random variables (case iii), underestimates the conditional failure probabilities (fragilities) compared to the case of stochastic distribution, especially for high values of the intensity measure where the structure approaches collapse. Moreover, the bridge fragilities are not affected by the correlation length, since the b=0.2 and b=10 curves, practically coincide.

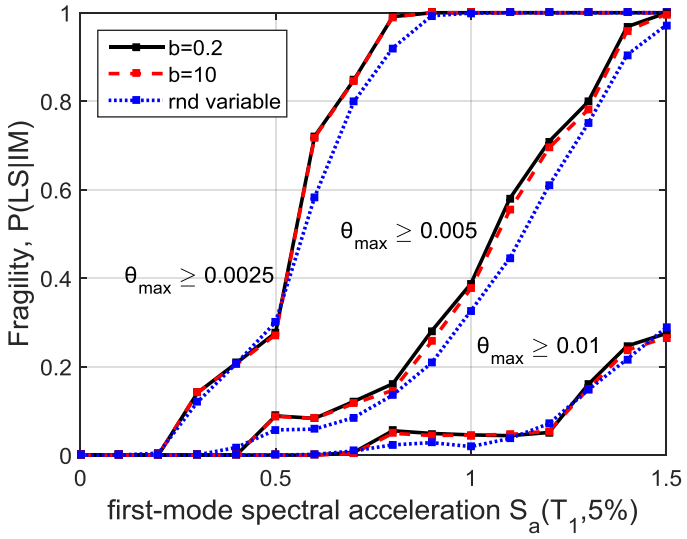

Figure 28: Fragility curves considering different values of the correlation length parameter

Often the response variability is counteracted and hence hidden when it is measured with a global demand parameter (Li *et al*. 2015). In other words, while in many cases the response variability in terms of displacements (or drifts) may be small, the variability in terms of local demand parameters can be more pronounced. For example, in the local level the demand and capacity are expressed in terms of curvature k_{max}. We, therefore, examine the curvature demand at the bottom of the shortest pier (Figure 26) and we produce the corresponding fragility curves. The fragility curves are compared in Figure 29 for the three cases previously discussed. Again the coupling of stochasticity and nonlinearity is strong for large seismic intensities. Contrary to Figure 28, the random variable case overestimates the fragility of the pier, while considerable variability between the *b*=0.2 and *b*=10 curves is also observed. It is therefore evident that the proper description of randomness significantly affects the response, although this may be hidden if global response parameters (EDPs) are studied instead.

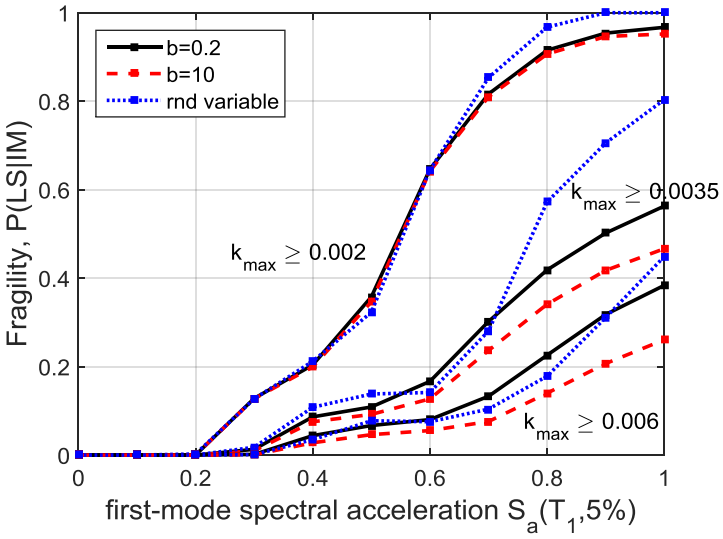

Figure 29: Single pier fragility curves for different values of the correlation length parameter.

7. Concluding remarks

A novel modeling approach for the probabilistic seismic assessment of frame structures with stochastic system properties is proposed. The proposed method extends the use of flexibility-based fiber elements to the stochastic finite element method, which now can be applied for the study of real-scale problems due to the remarkable computational performance and the stability of these elements. The performance of the proposed modelling is demonstrated on a one-storey steel portal frame and on a reinforced concrete bridge. The study provides a valuable guidance for the analysis and the design of structures with non-Gaussian system properties and its main conclusions are summarized as follows:

- The number of integration sections is critical. The integration should be able to capture the spectral characteristics of the input stochastic field.
- The proposed modelling combines remarkable accuracy and reduced computing effort, even for very small values of the correlation length parameter.
- The computational performance was exceptional, especially for the case of response history analysis where the proposed modelling reduced the required computing effort by 90% compared to ordinary displacement-based fiber elements.
- The parametric investigation revealed notable influence of the correlation scale of the stochastic parameters, especially for higher order statistical moments. The record-to-record variability for the dynamic response of the structures was found also very important.
- The influence of stochastic system properties grows as inelastic demand increases, i.e. for levels of high seismic intensity. The discrepancies of the probabilistic characteristics of the input, particularly the difference between the widely used

random variables and the stochastic fields, are clearly reflected through the fragility curves, even though the response variability is milder when it is measured globally. Therefore, local demand parameters (e.g. column/pier curvature) should be also studied in the framework of seismic reliability assessment.

- This page was left intentionally blank -

References

Bocchini, P., Deodatis, G. 2008. Critical Review and Latest Developments of a Class of Simulation Algorithms for Strongly Non-Gaussian Random Fields. Probabilistic Engineering Mechanics 23, p. 393-407.

Bowman, A.W., Azzalini, A., 1997. Applied Smoothing Techniques for Data Analysis. Oxford University Press, UK.

Ciampi, V., Carlesimo L., 1986. A Nonlinear Beam Element for Seismic Analysis of Structures. 8th European Conference in Earthquake Engineering, Lisbon, Portugal.

Coleman, J., Spacone, E., 2001. Localization Issues in Force-based Frame Elements. Journal of Structural Engineering 127(11), p. 1257-1265.

Der Kiureghian, A., Ke, J.B., 1988. The Stochastic Finite Element Method in Structural Reliability. Probabilistic Engineering Mechanics 3, p. 83-91.

Dymiotis, C., Kappos, A.J., Chryssanthopoulos, M.K., 1999. Seismic Reliability of RC Frames with Uncertain Drift and Member Capacities. Journal of Structural Engineering (ASCE) 125(9), p. 1038-1047.

Feng, D., Li, J., 2015. Stochastic Nonlinear Behavior of Reinforced Concrete Frames. II: Numerical Simulation. Journal of Structural Engineering (ASCE) DOI: 10.1061/(ASCE)ST.1943-541X.0001443.

Fragiadakis, M., 2016. Nonlinear Analysis of Steel and RC Frame Structures, Laboratory for Earthquake Engineering, Class notes, Athens, Greece.

Fragiadakis, M., Vamvatsikos, D., Karlaftis, M.G., Lagaros, N.D., Papadrakakis, M., 2014. Seismic Assessment of Structures and Lifelines. Journal of Sound and Vibration 334, p. 29-56.

Grigoriu, M., 1998. Simulation of Stationary Non-Gaussian Translation Processes. Journal of Engineering Mechanics (ASCE) 124(2), p. 121-126.

Hamutcuoglu, O.M., Scott, M.H., 2009. Finite Element Reliability Analysis of Bridge Girders considering Moment-Shear Interaction. Structural Safety 31, p. 356-362.

Hurtado, J.E., Barbat, A.H., 1998. Monte Carlo Techniques in Computational Stochastic Mechanics. Archives of Computational Methods in Engineering 5(1), p. 3-30.

Joint Committee for Structural Safety. Probabilistic Model Code. Part 3: Resistance Models, 2001.

Lee, T-H., Mosalam, M., 2004. Probabilistic Fiber Element Modeling of Reinforced Concrete Structures. Computers and Structures 82, p. 2285-2299.

Li, J., Feng, D., Gao, X., Zhang, Y., 2015. Stochastic Nonlinear Behavior of Reinforced Concrete Frames. I: Experimental Investigation. Journal of Structural Engineering (ASCE) DOI: 10.1061/(ASCE)ST.1943-541X.0001442.

MATLAB Release 2014b, The MathWorks, Inc., Natick, Massachusetts, United States.

Matthies, H.G., Brenner, C.E., Bucher, C.G., Guedes Soares, C., 1997. Uncertainties in Probabilistic Numerical Analysis in Structures and Solids – Stochastic Finite Elements. Structural Safety 19(3), p. 283-336.

McKenna, F., Fenves, G.L., 2001. The OpenSees Command Language Manual Version 1.2. Pacific Earthquake Engineering Research Centre, University of California, Berkeley.

Most, T., Bucher, C., 2006. Stochastic Simulation of Cracking in Concrete Structures Using Multiparameter Random Fields. International Journal of Reliability and Safety 1, p. 168-187.

Most, T., Bucher, C., 2007. Probabilistic Analysis of Concrete Cracking Using Neural Networks and Random Fields. Probabilistic Engineering Mechanics 22, p. 219-229.

Neuenhofer, A., Filippou, F., 1998. Geometrically Nonlinear Flexibility-Based Frame Finite Element. Journal of Structural Engineering (ASCE) 124(6), p. 704-711.

Papadrakakis, M., Papadopoulos, V., Lagaros, N.D., 1996. Structural Reliability Analysis of Elastic-Plastic Structures using Neural Networks and Monte Carlo Simulation. Computational Methods in Applied Mechanics and Engineering 136, p. 145-163.

Shields, M.D., Deodatis, G., 2013. A Simple and Efficient Methodology to Approximate a General Non-Gaussian Stationary Stochastic Vector Process by a

Translation Process with Applications in Wind Velocity Simulation. Probabilistic Engineering Mechanics 31, p. 19-29.

Shinozuka, M., 1972. Monte Carlo Solution of Structural Dynamics. Computers and Structures 2, p. 855-874.

Shinozuka, M., Deodatis, G., 1991. Simulation of Stochastic Processes by Spectral Representation. Applied Mechanics Reviews (ASME) 44(4), p. 191-203.

Spacone, E., Ciampi, V., Filipou, F., 1996. Mixed Formulation of Nonlinear Beam Element. Computers and Structures 58(1), p. 71-83.

Stefanou, G., 2009. The Stochastic Finite Element Method: Past, Present and Future. Computational Methods in Applied Mechanics and Engineering 198, p.1031-1051.

Stefanou, G., Fragiadakis, M., 2009. Nonlinear Dynamic Analysis of Frames with Stochastic Non-Gaussian Material Properties. Engineering Structures 31, p. 1841-1850.

Vasconcellos Real, M.d., Filho, A.M., Maestrini, S.R., 2003. Response Variability in Reinforced Concrete Structures with Uncertain Geometrical and Material Properties. Nuclear Engineering and Design 226, p. 205-220.

Zeris, C., Mahin, S.A., 1988. Analysis of reinforced concrete beam-columns under uniaxial excitation. Journal of Structural Engineering 114(4), p. 804–820.

- This page was left intentionally blank -

Appendix

Appendix A

Numerical Integration Rules

Table A.3: Gauss-Legendre quadrature

Number of integration points m	Points ξ_h	Weights w_h
1	0.0	2.0
2	± 0.57735	1.0
3	± 0.774597	0.555556
	0.0	0.888889
4	± 0.861136	0.347855
	± 0.339981	0.652145
5	± 0.90618	0.236927
	± 0.538469	0.478629
	0.0	0.568889
6	± 0.93247	0.171324
	± 0.661209	0.360762
	± 0.238619	0.467914
7	± 0.949108	0.129485
	± 0.741531	0.279705
	± 0.405845	0.38183
	0.0	0.417959

8	± 0.96029	0.101229
	± 0.796666	0.222381
	± 0.525532	0.313707
	± 0.183435	0.362684
9	± 0.96816	0.081274
	± 0.836031	0.180648
	± 0.613371	0.260611
	± 0.324253	0.312347
	0.0	0.330239
10	± 0.973907	0.066671
	± 0.865063	0.149451
	± 0.67941	0.219086
	± 0.433395	0.269267
	± 0.148874	0.295524

Table A.4: Gauss-Lobatto quadrature

Number of integration points m	Points ξ_h	Weights w_h
1	-	-
2	± 1.0	1.0
3	± 1.0	0.333333
	0.0	1.333333
4	± 1.0	0.166667
	± 0.447214	0.833333
5	± 1.0	0.1
	± 0.654654	0.544444
	0.0	0.711111
6	± 1.0	0.066667
	± 0.765055	0.378475
	± 0.285232	0.554858
7	± 1.0	0.047619
	± 0.830224	0.276826
	± 0.468849	0.431745
	0.0	0.487619
8	± 1.0	0.035714
	± 0.87174	0.210704
	± 0.5917	0.341123
	± 0.209299	0.412459

	± 1.0	0.027778
	± 0.899758	0.165495
9	± 0.677186	0.274539
	± 0.363117	0.346429
	0.0	0. 371519
	± 1.0	0.022222
	± 0.919534	0.133306
10	± 0.738774	0.224889
	± 0.477925	0.292043
	± 0.165279	0.327540

Appendix B

Matlab script for Gauss-Lobatto quadrature

```
% Gauss - Lobatto integration rule
% Calculation of locations and weights of integration points

clear all; clc;
format long

n = 20 ;          % number of integration points
syms x ;
x = solve(diff(legendreP(n-1,x)),x);
x = double(x);
x = real(x);
x = sort(x);

% locations & weights
x = [-1 x' 1];
w = 2./(n*(n-1)*(legendreP(n-1,x)).^2);

% transformation to the natural domain [0,1]
x = 0.5*(1+x)
w = 0.5*w
```

Appendix C

Matlab script for the Spectral representation method

```
% Stochastic field generation
% 1D-1V homogeneous zero-mean Gaussian random field
% Spectral representation method

clear all; clc;

% Spectral density function
syms s b k
SDF = (s^2*b)/(2*pi^0.5)*exp(-0.25*(b^2)*(k^2));
SDF = subs(SDF,s,0.1);          % input of standard deviation
SDF = subs(SDF,b,20);           % input of correlation length

% Generate 1000 sample functions of the random field
a=int(SDF);                     % symbolic integration of power spectrum
for i=1:1:1000                  % procedure for calculating the upper frequency
  b=double(limit(a,i));
  c=double(limit(a,inf));
  if (b/c)>0.999
    break
  end
end
wu=i;                           % upper cut frequency (power spectrum is practically
zero)
Sf=inline(char(SDF));           % convert sym to inline function
N=100;                          % truncation
Dw=wu/N;                        % frequency step
for j=1:1:1000
  for i=0:1:N-1
    wn=i*Dw;
    An=(2*Sf(wn)*Dw)^0.5;
    t=linspace(0,2*pi/Dw,300);
    z=(2^0.5)*An*cos(wn*t+2*pi*rand());
    f(i+1,:)=z;                 % place generated data in a Nx300 matrix
  end
  F_temp=sum(f);
  F(j,:)=F_temp;
end
```

Appendix D

OpenSees script for stochastic nonlinear static analysis of 2D portal frame

```
# Create ModelBuilder (with 2-dimensions and 3 DOF/node)
model basic -ndm 2

set height 6;
set width 8;
node 1 0 0
node 2 0 $height
node 3 $width $height
node 4 $width 0

# Fix supports
fix 1 1 1 1
fix 4 1 1 1

source Stoch_field.tcl

#Steel attributes (kN/m^2)
set fy 235e3;
set E 210e6;

set f [list $f1 $f2 $f3 $f4 $f5 $f6 $f7 $f8 $f9 $f10 \
      $f11 $f12 $f13 $f14 $f15 $f16 $f17    $f18 $f19 $f20]
set g [list $g1 $g2 $g3 $g4 $g5 $g6 $g7 $g8 $g9 $g10 \
      $g11 $g12 $g13 $g14 $g15 $g16 $g17 $g18 $g19 $g20]

for {set i 1} {$i <=20} {incr i} {
         set a [lindex $f $i-1]
         set b [lindex $g $i-1]
         lappend Elist [expr $E*(1+$a)]
         lappend fylist [expr $fy*(1+$b)]
}

# Bilinear material (S_235) law with hardening
# uniaxialMaterial Steel01 $matTag $Fy $E0 $b <$a1 $a2 $a3 $a4>
for {set i 1} {$i <=20} {incr i} {
         set a [lindex $Elist $i-1]
         set b [lindex $fylist $i-1]
         uniaxialMaterial Steel01 $i $b $a 0.000001
}
```

```
for {set i 1} {$i <=20} {incr i} {
        lappend sectag $i
}

# HEB 200
for {set i 1} {$i<=20} {incr i} {
        set a [lindex $sectag $i-1]
        section WFSection2d  $a  $i  0.2  0.009  0.2  0.015 15  5
}

geomTransf Corotational 1;       # beams
geomTransf Corotational 2;       # columns

# Gauss - Lobatto Integration
set locations "0   0.009628147553043   0.032032750593667   0.066561010955025  \
0.112315869523972   0.168111798854844   0.232503567984057  \
0.303823408143045   0.380224147038507   0.459727031380589  \
0.540272968619411   0.619775852961493   0.696176591856955  \
0.767496432015943   0.831888201145156   0.887684130476028  \
0.933438989044975   0.967967249406333    0.990371852446957   1.0"

set weights "0.002631578947368   0.016118561594244   0.028590901063783  \
0.040315881998060   0.050995749849725   0.060354613814337  \
0.068150241179362   0.074180777035458   0.078290051323738  \
0.080371643193923   0.080371643193923   0.078290051323738  \
0.074180777035458   0.068150241179362   0.060354613814337  \
0.050995749849725   0.040315881998060   0.028590901063783  \
0.016118561594244   0.002631578947368"

set sectags "1 2 3 4 5 6 7 8 9 10 11 12 13 14 15 16 17 18 19 20";

set np 20;
set integration "UserDefined $np $sectags $locations $weights";

# element forceBeamColumn $eleTag $iNode $jNode $transfTag "IntegrationType”
element forceBeamColumn        1       1       2       2       $integration
element forceBeamColumn        2       2       3       1       $integration
element forceBeamColumn        3       3       4       2       $integration

# Set gravity load
set gravityLoad [expr -80];     # kN
```

```
# Define constant Gravity load
pattern Plain 1 "Constant" {
    # nodetag    load value 3 DOF (x,y,θ)
        load         2     0 $gravityLoad 0
        load         3     0 $gravityLoad 0
}

# Define analysis parameters
initialize
system SparseGeneral -piv
test NormUnbalance 1.0e-4 10000
numberer Plain
constraints Plain
algorithm Newton

# Create recorders
recorder Node -file Fdisp20.txt -time -node 3 -dof 1 disp

# Set horizontal load
set horizontalLoad 1
pattern Plain 2 "Linear" {
        load 2 $horizontalLoad 0 0
}

set numIncr 300;
set maxdisp 0.25;
# integrator DisplacementControl $node $dof              $incr
integrator DisplacementControl        3       1   [expr $maxdisp/$numIncr]
analysis Static
set ok [analyze $numIncr];

if {$ok == 0} {
        puts "Pushover analysis completed SUCCESSFULLY";
}
else {
        puts "Pushover analysis FAILED";
}

set fileErr [open err.txt w]
puts $fileErr "$ok"
close $fileErr;
```

- This page was left intentionally blank -